UNIVERSITY OF CALIFORNIA,
IRVINE

Computational Models of Virus Dynamics

DISSERTATION

submitted in partial satisfaction of the requirements
for the degree of

DOCTOR OF PHILOSOPHY

in Ecology and Evolutionary Biology

by

Sarah Marie Roy

Dissertation Committee:
Professor Dominik Wodarz, Chair
Associate Professor Robin Bush
Associate Professor Kevin Thornton

2015

DEDICATION

To my parents
and to Hans, in loving memory

TABLE OF CONTENTS

LIST OF FIGURES

ACKNOWLEDGMENTS

I would like to thank my thesis advisor Dominik Wodarz, for his support and guidance throughout graduate school.

I would like to thank my committee members Robin Bush and Kevin Thornton, for their valued input and perspectives.

I'd like to thank all the faculty and staff of the Ecology and Evolutionary Biology program at UC Irvine for fostering my education.

Finally, I want to thank the EEB grads for the great memories.

CURRICULUM VITAE

Sarah Marie Roy

2010	B.S. in Biological Sciences, University of California, Irvine
2010	Research Assistant, Ecology and Evolutionary Biology, University of California, Irvine
2011	Graduate Student Researcher, Ecology and Evolutionary Biology, University of California Irvine
2011-2015	Teaching Assistant, Ecology and Evolutionary Biology, University of California, Irvine
2015	Ph.D. in Ecology and Evolutionary Biology, University of California, Irvine

FIELD OF STUDY

Mathematical and Computational Biology

PUBLICATIONS

Roy, S.M., and Wodarz, D. 2012. Infection of HIV-specific CD4 T helper cells and the clonal composition of the response. J Theor Biol. 304: 143-151

Roy, S.M., and Wodarz, D. 2014. Tissue architecture, feedback regulation, and resilience to viral infection. J Theor Biol. 340:131-138

ABSTRACT OF THE DISSERTATION

Computational Models of Virus Dynamics

By

Sarah Marie Roy

Doctor of Philosophy in Ecology and Evolutionary Biology

University of California, Irvine, 2015

Professor Dominik Wodarz, Chair

The following thesis explores the within-host population dynamics of viruses and their target cells using mathematical and computational models. Chapter 1 investigates the dynamics that arise when two independently regulated HIV-specific t helper cell populations grow by clonal expansion in response to antigenic stimulation by HIV. Despite no direct competition for antigenic stimulation, we find that it is still possible for the stronger clone to drive the weaker clone to extinction through the process of apparent competition. In addition, we find that under certain conditions a weaker clonal population can be facilitated by the presence of a stronger one, causing the weaker clone to become established where it would have failed to persist in isolation. Chapter 2 explores the regulation of tissue architecture in a model of stem cells and differentiated cells. We investigate two types of feedback regulation, and discuss how these regulatory controls influence the ability to maintain tissue homeostasis during viral infections. We find that when feedback factors are produced by stem cells, viral infection leads to a significant reduction in the number of differentiated cells (tissue pathology), while the number of stem cells is not affected at equilibrium. In contrast, if the feedback factors are produced by

differentiated cells, a viral infection never reduces the number of tissue cells at equilibrium because the feedback mechanism compensates for virus-induced cell death. However, the number of stem cells becomes elevated, which could increase the chance of these stem cells to accumulate mutations that drive cancer. In Chapter 3, we investigate viral infection in an agent-based model, allowing us to simulate in-host microenvironments that have some spatial structure, such as the lymph nodes. The model explores the consequences of multiple infection and an increased burst size on the dynamics of early viral spread through host cells. We find that the model predicts larger proportions of multiply infected cells at low viral loads in environments where mobility is limited. In addition, when an increased burst size in multiply infected cells is included in the model, both accelerated viral spread and a decreased probability of infection extinction are observed.

INTRODUCTION

This dissertation explores the ecology of viruses and their target cell populations using mathematical and computational models that investigate different aspects of these within-host disease dynamics. Viruses and their host cells are treated as interacting groups of organisms, with the goal of gaining insights into the principles governing the population dynamics of viral infections. There is a growing body of research in the field of mathematical biology that explores the dynamics of Human Immunodeficiency Virus (HIV) infection. HIV is characterized by large numbers of complex interactions with multiple immune cell types, as well as a high mutation rate that drives rapid viral evolution. Much of our current understanding of how infection plays out comes from patient data, which provide a limited snapshot of the underlying disease dynamics. Mathematical and computational models help us investigate these largely unobservable interactions, generating testable predictions that motivate clinical and experimental studies. Models also give us insight into the principles governing infection, linking theoretical understanding to experimental outcomes and patient data.

HIV- Overview

In the early 1980's, hospitals began reporting an increased incidence of opportunistic infections and rare cancers in clustered populations of gay men and intravenous drug users. By 1984, researchers had identified the causative agent of this new disease- a retrovirus that targeted the immune system, first misclassified as a new strain of

human T-lymphotropic virus (HTLV). The virus was named HTLV-III in the U.S. and lymphadenopathy-associated virus (LAV) in France. Soon after, the molecular structure and link between the newly discovered virus and acquired immune deficiency syndrome (AIDS) were established, and HTLV-III/LAV was renamed human immunodeficiency virus (HIV).

There are 37 million people worldwide living with HIV as of 2015, with 1.2 million of those infected individuals residing in the U.S (UNAIDS). The largest AIDS epidemic by country is in South Africa, where 6.8 million individuals (about 12% of the total population) are infected, with 340,000 individuals newly infected each year. There are numerous socioeconomic obstacles to treating the HIV epidemic in developing countries that lack adequate government infrastructure, and access to public health care and testing remains foremost among these issues in many areas. Public attitudes, including AIDS denialism and the lingering stigma of HIV as a "homosexual" disease, are further barriers to diagnosing and treating millions of infected individuals in these developing countries. It is estimated that 19 million infected individuals worldwide were unaware of their HIV-positive status (UNAIDS).

HIV Structure and Life Cycle

HIV is in the family of retroviruses, a group of RNA viruses whose life cycle includes a DNA intermediate produced by the viral enzyme reverse transcriptase. The enveloped virus is pseudodiploid- each virion is packaged with two complete copies of the positive-sense single stranded RNA genome. The genome also comes packaged with several viral

proteins that aid in transcription and integration into the host cell. The CD4+ receptor, which is present on the surface of several types of immune cells, is the access point for HIV. The virus uses a co-receptor, typically either CCR5 or CXCR4, to assist with viral entry across the host plasma membrane (Bleul et al., 1997). CCR5 is the primary co-receptor that HIV uses, and individuals who possess the CCR5-Δ32 mutation are resistant to infection (Liu et al., 1996). There are seven major stages in the life cycle of HIV, from entry to release of new virus particles from the host. Assuming that infection occurs via free virus transmission, the replication cycle begins with binding of virus to CD4+ receptors on the surface of target cells. Fusion of the viral envelope with the cell membrane releases viral contents into the cytoplasm of the cell. The viral enzyme reverse transcriptase constructs a single stranded DNA copy of the viral genome in the cytoplasm by jumping between the two single-stranded RNA genomes. This process is highly error prone, on the order of 10^{-5} substitutions per base pair per replication cycle (Mansky and Temin, 1995). The completed DNA genome migrates to the nucleus of the cell, where it is inserted into the host genome with the help of the viral enzyme integrase. The integrated viral genome is known as a provirus. The integrated provirus will either lie dormant, leading to a latently infected cell that may eventually activate, or it will begin producing the next generation of virus particles. During viral production the host transcriptional machinery is used to produce viral mRNA, which is spliced and sent to the cytoplasm for assembly. In the cytoplasm, immature new virions are packaged and undergo “budding”- packaged virus leave the host cell, pinching off parts of the host’s lipid membrane to form new viral envelopes. Budding virions must undergo maturation in order to become infectious, a process which involves

cleaving and folding of viral proteins into their final functional states (Sundquist and Krausslich, 2012).

HIV targets several different types of cells within the immune system that are found throughout the body. The main targets of HIV are the short-lived activated CD4+ T cells of the adaptive immune system (Douek et al, 2002). When productively infected, these cells turn over rapidly, with a half-life of about 2 days (Ho et al, 1995; Wei et al, 1995). Infection of resting (non-activated) CD4+ T cells typically results in latent rather than productive infection (Siliciano and Greene, 2011), and cells in this state have a half-life of 44 months (Pierson et al, 2000). Other targets of HIV infection include dendritic cells and macrophages, immune cells of the innate immune system that also express the CD4+ surface protein required for HIV entry.

HIV- Stages of Infection

Untreated HIV infection proceeds in three distinct phases. The first phase, the acute phase, occurs during the first 3-6 months following contraction of the virus and is often accompanied by flu-like symptoms. Circulating CD4+ T cells rapidly drop, while plasma virus levels increase exponentially and peak around 21-28 days following infection, eventually declining to a viral set point of about 10^3-10^5 virions/ml (O'Brien and Hendrickson, 2013), (McMichael et al, 2010). It is during this acute period that the virus is rapidly disseminated throughout the body and a large reservoir of latently infected cells becomes established. This is also the period during which the adaptive immune response begins to mount a defense against the virus. Following the acute phase of infection, the

chronic or asymptotic phase of infection typically lasts between 5-10 years. The chronic period of infection is characterized by a low viral load but a high rate of viral turnover, i.e. the virus is still actively infecting and replicating but is mostly controlled by the continuously active immune system (Pantaleo et al, 1993). Left untreated, HIV will ultimately deplete the CD4+ population to below 200 cells/mm^3, at which point the disease has progressed to AIDS. The weakened immune system is highly vulnerable to opportunistic infections, and AIDS-related mortality is associated with these complications.

HIV Treatment

There is no cure or vaccine for HIV. One of the greatest obstacles to curing HIV infection is the high mutation rate of the virus combined with a rapid turnover rate. Mutants are generated at the rate of 3×10^{-5} per base pair per replication cycle, with about 10^{10} new virions produced per day. Thus, millions of viral variants are generated in a single host each day. This allows the virus to continuously mutate away from detection by the immune system, and is also responsible for the rapid rise of single-drug resistant viral strains. Another obstacle to eradicating HIV from the body is the reservoir of latently infected immune cells, such as resting CD4+ T cells, which are very long lived. Cells harboring integrated provirus are frequently undetectable by the host immune system, and are capable of activation and production of new virus.

HIV infected individuals are treated using antiretroviral therapy (ART), which is a 3-drug combination that typically includes two reverse transcriptase inhibitors and a protease inhibitor. Using a "cocktail" of drugs inhibits viral load to nearly undetectable

levels, ensuring that there is no likelihood of generating a viral mutant resistant to all three drugs in the lifetime of the patient. Lack of adherence to drug therapy in an infected individual leads to rapid expansion of the viral population, and sustained viral suppression is one of the best predictors of long-term disease control during ART (Wit et al., 1999)

In 2012, the FDA approved the antiretroviral combination drug Truvada as an HIV pre-exposure prophylactic (PrEP). Originally indicated for use in HIV ART treatment, Truvada can also prevent HIV infection when taken regularly for several days prior to exposure, and a similar drug combination is used as a post-exposure prophylactic or PEP (Grant et al., 2010; Winston et al., 2005). Retroviral treatments like ART and PrEP/PEP require close adherence to the treatment regime to be effective. Short-term adherence is often difficult due to unpleasant side effects such as nausea, and antiretrovirals have significant long-term side effects associated with their toxicity as well, including bone density loss and liver damage (Nunez, 2006; Pan et al., 2006).

Mathematical Modeling of Virus Dynamics

This thesis explores the interactions between virus and host cell interactions at the population level. Population dynamics models are a critical component to the study of virology, as the ability to formulate equations that accurately predict biological outcomes can provide insight into the underlying dynamics of the complex interactions between viruses and the immune system. Mathematical descriptions of viral dynamics have been vital to the understanding of antiviral therapies, viral evolution, and to our understanding of viral pathogenesis (Perelson, 2002; Perelson and Ribeiro, 2013). These models, when

combined with data from *in vitro* experiments, allow us to better describe processes that are often impossible to experimentally test in humans, and prohibitively expensive to investigate in animals. The collaboration between mathematical and experimental scientists since the 1990's has resulted in several important breakthroughs that have come to define the field, including estimates of key parameters such as infected cell death rate (Nowak and May, 2000; Perelson and Ribeiro, 2013).

The population dynamics of viral infections can be formulated as a system of differential equations that describes the process of infecting cells to produce new virus. The basic model of virus dynamics as formulated by Nowak and May serves as a starting point for numerous published modeling works that describe how viruses and their target cells interact, including the first and third chapters of this thesis.

There are three populations in the basic model: x, uninfected cells, v, free virus, and y, infected cells. Uninfected cells are assumed to be produced at a constant rate λ, and these cells die at rate dx. Free virus particles decay at rate uv. Free virus particles encounter and infect uninfected cells at rate βxv. Note that the infectivity parameter β also encompasses the "handling time" of successful viral fusion and entry. Infected cells produce free virus with rate ky, and die with rate ay. It is assumed that $a > d$ in this model, i.e. infected cells decay more rapidly than uninfected cells. This model can be formulated as a system of differential equations shown below:

$$\dot{x} = \lambda - dx - \beta xv$$

$$\dot{y} = \beta xv - ay$$

$$\dot{v} = ky - uv$$

In the basic model of virus dynamics, establishment of infection is predicted by R_0, the basic reproductive ratio of the infection or basic reproductive rate. R_0 is defined as the total number of newly infected cells that arises from one singly infected cell when most cells are uninfected. The formulation of this ratio is found by dividing all such parameters that promote the spread of infection, including β, by all such parameters that inhibit the spread of infection, including the decay rate of free virus, u. This gives us the following ratio:

$$R_0 = \lambda\beta k/dau$$

This ratio is useful because it predicts if a new infection will "take hold" and spread, or decline to extinction. If $R_0<1$, the infection will not become established, as each infected cell is on average leading to less than one newly infected cell and the population will decay. If R_0 is greater than 1, infection is established in this deterministic model. Both virus, v, and infected cells, y, will grow exponentially and peak, then decline to an equilibrium value given by the following steady-state solutions:

$y^* = (R_0 - 1)du/\beta k,$

$v^* = (R_0 - 1)d/\beta$

Uninfected cells will decline from a pre-infection load of $x_0 = \lambda/d$ to the steady-state infection equilibrium:

$x^* = x_0/R_0$

The formulation of the basic model of virus dynamics has provided numerous insights into the underlying principles governing interacting populations of viruses and their host cells. In the case of HIV, a modified version of the above model has been used to accurately predict the decay rate of free virus in the blood after the onset of drug treatment (Nowak

and May 2000). This model has also been shown to accurately describe the kinetics of the acute phase of HIV infection (Stafford et al 1999).

The three chapters of this thesis explore models of virus dynamics in several different contexts. Chapter 1 investigates competitive and facilitative interactions between multiple HIV CD4+ T cell populations during the acute phase of HIV infection, before a significant immune defense has been mounted. Chapter 2 explores the regulatory mechanisms that contribute to the stable growth and division of stem cell lineages, and how these mechanisms respond during a challenge to feedback control- in this case, viral infection of the stem cell lineage. Chapter 3 explores the consequences of multiple infection in host cells on the dynamics of viral spread in a spatially limited environment.

References:

Anon. 2014. The UNAIDS Gap report. The Joint United Nations Programme on HIV/AIDS (UNAIDS).

Bleul, C.C., L. Wu, J.A. Hoxie, et al. 1997. The HIV coreceptors CXCR4 and CCR5 are differentially expressed and regulated on human T lymphocytes. Proc Natl Acad Sci USA 94(5):1925-1930

Douek, D.C., J.M. Brenchley, M.R. Betts, D.R. Ambrozak, B.J. Hill, Y. Okamoto, J.P. Casazza, J. Kuruppu, K. Kunstman, S. Wolinsky, Z. Grossman, M. Dybul, A. Oxenius, D.A. Price, M. Connors, and R.A. Koup. 2002. HIV preferentially infects HIV-specific CD4+ T cells. Nature, 417:95–98

Grant, R.M., J.R. Lama, P.L. Anderson, et al. 2010. Preexposure chemoprophylaxis for HIV prevention in men who have sex with men. NE J Med 363(27):2587-99

Ho, D.D., A.U. Neumann, A.S. Perelson, W. Chen, J.M. Leonard, and M. Markowitz. 1995. Rapid turnover of plasma virions and Cd4 lymphocytes in Hiv-1 infection. Nature 373:123–126

Liu, R., W.A. Paxton, S. Choe, et al. 1996. Homozygous Defect in HIV-1 Coreceptor Accounts for Resistance of Some Multiply-Exposed Individuals to HIV-1 Infection. Cell. 86(3):367-77

Mansky, L.M. and Temin, H.M. 1995. Lower in vivo mutation rate of human immunodeficiency virus type 1 than that predicted from the fidelity of purified reverse transcriptase. J Virol 69(8): 5087–5094

McMichael, A.J., P. Borrow, G.D. Tomaras, et al. 2010. The immune response during acute HIV-1 infection: clues for vaccine development. Nature Rev Immunol 10:11-23

Nowak, M.A.and May, R.M. Virus Dynamics. Oxford University Press, 2000.

Nunez, M. 2006. Hepatotoxicity of antiretrovirals: Incidence, mechanisms and management. J Hepatology 44(S1):S132-139

Pan., G., Z. Yang, S.W. Ballinger, and J.M. McDonald. 2006. Pathogenesis of Osteopenia/Osteoporosis Induced by Highly Active Anti-Retroviral Therapy for AIDS. Ann NY Acad Sci 1068:297-308

Perelson, A.S. and R.M. Ribeiro. 2013. Modeling the within-host dynamics of HIV infection. BMC Biol 11:96

Pierson, T. McArthur, J., and Siliciano, R.F. 2000. Reservoirs for HIV-1: mechanisms for viral persistence in the presence of antiviral immune responses and antiretroviral therapy. Annu Rev Immunol. 18:665-708

Siliciano, R.F. and Greene, W.C. 2011. HIV Latency. Cold Spring Harb Perspect Med 1(1)

Stafford, M., L. Corey, Y. Cao, E.S. Daar, D.D. Ho, and A.S. Perelson. 2000. Modeling Plasma Virus Concentration during Primary HIV Infection. J Theor Biol 203:285-301

Sundquist, W.I. and Krausslich, H.G. 2012. HIV-1 Assembly, Budding, and Maturation. Cold Spring Harbor Perspect Med 2(7)

Wei, X.P., S.K. Gosh, M.E. Taylor et al., 1995. Viral dynamics in human-immunodeficiency-virus type-1 infection. Nature 373(6510):117–122

Winston, A., J. McAllister, J. Amin, D.A. Cooper, and A. Carr. 2005. The use of a triple nucleoside-nucleotide regimen for nonoccupational HIV post-exposure prophylaxis. HIV Med 6(3):191-197

Wit, F.W., R. van Leeuwen, G.J. Weverling, et al. 1999. Outcome and Predictors of Failure of Highly Active Antiretroviral Therapy: One-Year Follow-Up of a Cohort of Human Immunodeficiency Virus Type 1-Infected Persons. J Inf Dis 179 (4):790-798

Chapter 1: Infection of HIV-specific CD4 T helper cells and the clonal composition of the response

Abstract

A hallmark of human immunodeficiency virus is its ability to infect CD4+ T helper cells, thus impairing helper cell responses and consequently effector responses whose maintenance depends on help (such as killer T cells and B cells). In particular, the virus has been shown to infect HIV-specific helper cells preferentially. Using mathematical models, we investigate the consequence of this assumption for the basic dynamics between HIV and its target cells, assuming the existence of two independently regulated helper cell clones, directed against different epitopes of the virus. In contrast to previous studies, we examine a relatively simple scenario, only concentrating on the interactions between the virus and its target cells, not taking into account any helper-dependent effector responses. Further, there is no direct competition for space or antigenic stimulation in the model. Yet, a set of interesting outcomes is observed that provide further insights into factors that shape helper cell responses. Despite the absence of competition, a stronger helper cell clone can still exclude a weaker one because the two clones are infected by the same pathogen, an ecological concept called “apparent competition”. Moreover, we also observe “facilitation”: if one of the helper cell clones is too weak to become established in isolation, the presence of a stronger clone can provide enhanced antigenic stimulation, thus allowing the weaker clone to persist. The dependencies of these outcomes on parameters is explored. Factors that reduce viral infectivity and increase the death rate of infected cells promote

coexistence, which is in agreement with the observation that stronger immunity correlates with broader helper cell responses. The basic model is extended to explicitly take into account helper-dependent CTL responses and direct competition. This study sheds further light onto the factors that can influence the clonal composition of HIV-specific helper cell responses, which has implications for the overall pattern of disease progression.

Introduction

Human immunodeficiency virus-1 (HIV-1) infection typically progresses through three phases: the acute phase in which extensive initial virus growth is observed that is eventually down-regulated; the chronic or asymptomatic phase during which virus load remains relatively low and the patient appears healthy; and the AIDS phase during which virus load rises sharply and destroys the CD4 T helper cell population to a degree at which the immune system effectively ceases to function. The dynamics between HIV-1 replication and immune responses has been subject to much research, both experimentally and mathematically (Douek et al., 2003, Nowak and May, 2000, Perelson, 2002 and Simon and Ho, 2003). This has provided many insights not only into patterns of disease progression but also into aspects of therapy. A characteristic that sets HIV infection apart from many other viral infections is the ability of the virus to impair not only the immune system as a whole, but also HIV-specific immune responses in particular (Kalams and Walker, 1998, Rosenberg and Walker, 1998, Rosenberg et al., 1997 and Rosenberg et al., 2000). Moreover, the ability of HIV to evolve rapidly in vivo (Ho et al., 1995, Mansky and Temin, 1995, Nowak, 1990 and Wei et al., 1995) allows the virus to escape immune responses that are

mounted by the patient (Goulder and Walker, 1999, Goulder et al., 1997, Goulder et al., 2001, Klenerman et al., 2000, McMichael and Phillips, 1997, Phillips et al., 1991 and Price et al., 1997). These aspects significantly contribute to the inability of the immune response to control the infection in the long term, eventually leading to uncontrolled viral replication and the development of AIDS.

HIV-1 infects a variety of cell types, including CD4+ helper T cells, macrophages, and dendritic cells, all of which play central roles in the establishment of immune effector responses, such as cytotoxic T lymphocyte (CTL) and B cell responses. Infection of these cells is the basis for virus-induced immune impairment, the dynamics of which has been analyzed in detail mathematically and experimentally (El-Far et al., 2008, Kalams and Walker, 1998, Komarova et al., 2003, Korthals Altes et al., 2003, Lifson et al., 2000, McLean and Kirkwood, 1990, Moir et al., 2011, Rosenberg and Walker, 1998, Rosenberg et al., 1997, Rosenberg et al., 1999, Rosenberg et al., 2000, Wodarz and Nowak, 1999, Wodarz and Jansen, 2001, Wodarz and Hamer, 2007 and Wodarz et al., 2000). Experiments have shown that HIV-specific helper cell infection not only occurs, but occurs preferentially over infection of T cells with other specificities (Douek et al., 2002 and Douek et al., 2003). This makes intuitive sense because HIV-specific T cells are likely to be abundant in anatomical areas that contain HIV-infected cells, allowing transmission to occur not only via free virus, but also from cell to cell through virological synapses (Hubner et al., 2009).

This study extends previous work and examines the dynamics of virus replication in HIV-specific helper T cell responses assuming the existence of two helper cell clones rather than one. We examine the consequences of HIV-specific helper cell infection for the dynamics and the clonal composition of the helper cell response in the simplest setting,

assuming no competition between the helper cell clones and the absence of helper-dependent effector responses. Interestingly, the model suggests that even in this simple setting, relatively complex dynamics are observed that can shape the early composition of the HIV-specific T helper cell response and that can therefore have lasting consequences for progression of the disease (Lifson et al., 1997). The effect of competition between helper cell clones and the presence of helper-dependent effector responses are subsequently studied in extensions of the basic model.

Basic dynamics of HIV-specific helper cell infection

We discuss a basic model that describes HIV dynamics in HIV-specific CD4+ T helper cells, assuming only a single helper cell population. This will form the basis for a more complex model that takes into account two helper cell clones, directed against different epitopes of the virus. Besides the specific helper cells, the model also takes into account an alternative target cell population, which can include non-specific helper cells as well as macrophages and dendritic cells. We denote uninfected and infected non-specific target cells by S and I, respectively. Uninfected and infected specific helper cells are denoted by x and y, respectively. The free virus population is denoted by v. The model is given by the following set of ordinary differential equations that describe the average time course of the infection:

(Eq. 1.1)

$$\frac{dx}{dt} = \frac{rxv(\gamma+\epsilon)(\gamma+\eta)}{(x+y+\epsilon)(v+\eta)} - dx - \beta xv$$
$$\frac{dy}{dt} = \beta xv - ay$$
$$\frac{dS}{dt} = \lambda - d_{ns}S - \beta_{ns}Sv$$
$$\frac{dI}{dt} = \beta_{ns}Sv - a_{ns}I$$
$$\frac{dv}{dt} = ky + k_{ns}I - uv$$

The HIV specific helper cells proliferate upon contact with virus with a rate r. While at relatively low virus load, the T cell proliferation rate is proportional to the amount of virus, v, this dependency saturates at higher virus loads. Further, the T cell proliferation term saturates as the overall number of specific T cells (x+y) grows, implying a regulatory mechanism that prevents unbounded growth of the immune response. The degree of saturation is given by the parameters ε and η. They also appear in the numerator of the expression such that large values of ε and η do not reduce the proliferation term and require rescaling of r. Upon contact with virus, the specific helper cells become infected with a rate β, and infected helper cells die with a rate a. Non-specific target cells are produced with a rate λ, die with a rate d_{ns}, and become infected upon contact with virus at a rate β_{ns}. Infected non-specific cells die with a rate ans. Virus is produced by specific and non-specific infected cells with a rate k and k_{ns}, respectively. Finally, free virus decays with a rate u. In this notation, the subscript "ns" stands for non-specific.

Note that the model is phenomenological in nature, describing complex biological processes with relatively simple terms. As mentioned above, the non-specific target cell population contains a group of cells consisting of T cells, dendritic cells and macrophages. In the equations, they are assumed to be produced with a constant rate λ. This might be a

correct assumption in general, but T cells are also likely to undergo cell divisions, which is not captured in the model. Hence, the rate λ should be considered to be a general input term and it is difficult to relate it to a particular process, the kinetics of which could be measured. On the other hand, the equation for the specific T cells ignores a constant production term assuming that significant increases in this population are driven mainly by antigen-induced cell division, as has been done in previous immune response models (Antia et al., 2005, Nowak and May, 2000 and Wodarz, 2006). A production term can significantly impact the dynamics if the number of immune cells is very low, further explored in Fig. 1.2.

This model is very similar to previous work that incorporated HIV-specific helper cells into mathematical models of HIV infection (Wodarz and Hamer, 2007). Specifically, their model only differed in the term that describes the proliferation of HIV-specific T cells, which was still antigen-driven, but limited through logistic growth. This was altered in the current study to include the more realistic assumption of saturated T cell proliferation. The paper by Wodarz and Hamer (2007) also considered antigen-driven expansion of infected HIV-specific helper cells. This was not included in the current model because its relevance is unclear given the relative short life-span of infected cells. Additionally, including this assumptions leads to biologically dubious outcomes, such as 100% prevalence of the virus in the T helper cell population (Wodarz and Hamer, 2007).

Model properties are summarized as follows. Because of the strong similarity of this model and its properties to the one analyzed in Wodarz and Hamer (2007), this section is designed to be more of an overview than a full analysis. For details, the reader is referred to Wodarz and Hamer (2007). The outcomes of the model include failure to establish a virus

infection; successful infection in the absence of a specific helper cell response; and establishment of infection in the presence of specific helper cells. It is useful to define the basic reproductive ratio of the virus (Nowak and May, 2000) in the non-specific target cells only, given by $R_0 = \frac{\lambda \beta_{ns} k_{ns}}{d_{ns} a_{ns} u}$. If $R_0>1$, then the virus can establish an infection in the non-specific target cells alone and can therefore persist. If the T cell response does not become established, the system converges to the following equilibrium: $S^* = \frac{u a_{ns}}{\beta_{ns} k_{ns}}$, $I^* = \frac{\lambda \beta_{ns} k_{ns} - d_{ns} a_{ns} u}{\beta_{ns} k_{ns} a}$, $v^* = \frac{\lambda \beta_{ns} k_{ns} - d_{ns} a_{ns} u}{\beta_{ns} a_{ns} u}$, $x^* = 0$, $y^* = 0$.

On the other hand, if the helper cell response does become established, the system converges to a different steady state at which all populations are greater than zero. This is given by the solution of a fourth degree polynomial and is thus not written out here.

Whether the specific T cell response is established can depend both on model parameters and on the initial conditions. Since the model does not include a production term for specific helper cells, the initial number of helper cells must be greater than zero for this population to expand in response to antigenic stimulation. If this is the case, the specific T cell response always becomes established if $((rv^*(\gamma+\epsilon)(\gamma+\eta))/(\epsilon(v^*+\eta))) - \beta_{ns} v^* - d > 0$, i.e. if the rate of antigen-induced proliferation is greater than the combination of the natural death rate and virus-induced impairment of the response. This condition is not fulfilled if the amount of stimulating virus, v^*, either lies below a threshold or above a threshold. If virus load is too low, it is insufficient to stimulate the response. If it is too high, the degree of immune impairment outweighs the degree of antigenic stimulation. This balance between immune stimulation in immune impairment

has been described before (e.g. Wodarz et al., 2000 and Younes et al., 2007). If the inequality does not hold, the specific helper cell response may or may not become established depending on the initial conditions (Fig. 1.1). A high initial virus load and a high initial number of specific helper cells can promote establishment of the helper cell response. It generates more infected cells, which in turn can provide higher levels of stimulation, thus leading to positive feedback. This dependence on initial conditions does, however, not occur in the entire parameter region in which the above inequality is not fulfilled. If the rate of helper cell expansion is too weak relative to the rate of loss, then the only outcome is failure of the response. This was determined by numerical simulations, and an analytic condition could not be obtained. This is explored more extensively in the study by Wodarz and Hamer (2007).

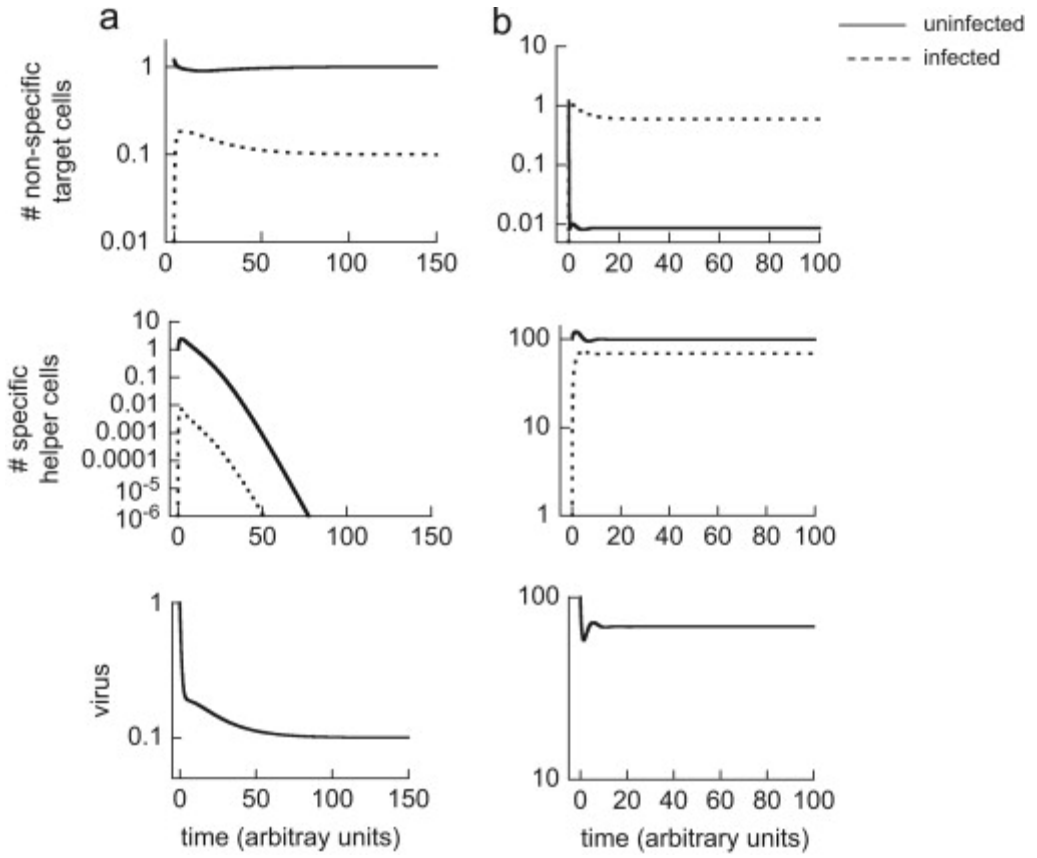

Fig. 1.1 Properties of model (1) assuming a single helper cell clone, demonstrating the dependence of the outcome on initial conditions. (a) Simulations are started with a low initial virus load and a low initial number of virus-specific helper cells, leading to the extinction of the specific helper cell response. (b) Simulations are started with a high initial virus load and a high initial number of virus-specific helper cells, leading to the persistence of the specific helper cell response. Note, this we consider this outcome biologically unrealistic because it requires most infected cells to be specific helper cells. Nevertheless, it is explored for completeness and parameters are chosen arbitrarily for illustrative purposes: β=0.01; d=0.5; a=1; r=2; ε=10; η=10; γ=1; k=1; u=1; βns=0.2; λ=0.12; d_{ns}=0.1; a_{ns}=0.2 k_{ns}=1. S(0)=λ/d_{ns}; I(0)=0; y(0)=0. (a) x(0)=1; v(0)=1 and (b) x(0)=100; v(0)=100.

Now assume that the basic reproductive ratio of the virus in the non-specific cells alone is less than one (R_0<1), i.e. an infection cannot be established in the non-specific cells alone. We observe the same dependence of outcome on initial conditions as before, i.e. a high initial virus load and a high initial helper cell population can lead to the establishment of the infection. In this case, the helper cell response obviously is established, and the virus

is present in both specific and non-specific target cells. Again, if the rate of helper cell expansion is too weak relative to the rate of loss, then the infection can never be established.

We note that the cases in which the establishment of the specific helper cell response depends on the initial conditions (beyond the trivial requirement that $x_0>0$) are not likely to be biologically realistic. It requires that the majority of virus replication occurs in specific helper cells rather than in non-specific target cells. In reality, however, infected specific helper cells make up about 1–10% of all infected cells in the blood (Douek et al., 2002), and the non-specific helper cells are thought to act in part as reservoirs that contribute to the maintenance of the virus in the host. Because the described dynamics are a property of the model, however, they are still important to discuss, and Fig. 1.1 does not rely on any measured parameters and is shown for illustrative purposes only.

While these insights are conceptually not novel (Wodarz and Hamer, 2007), this model provides the foundation for incorporating two specific helper cell clones in which the virus can replicate, described in the following section.

Infection dynamics in two helper cell clones

Here, we add a second helper cell clone to the model, directed against a different viral epitope. We denote clone 1 by subscript 1, and clone two by subscript 2. It is assumed that the two clones only differ in their proliferation rates, r_1 and r_2. The equations thus become

(Eq. 1.2)

$$\frac{dx_1}{dt} = \frac{r_1 x_1 v(\gamma+\epsilon)(\gamma+\eta)}{(x_1+y_1+\epsilon)(v+\eta)} - dx_1 - \beta x_1 v$$
$$\frac{dy_1}{dt} = \beta x_1 v - a y_1$$
$$\frac{dx_2}{dt} = \frac{r_2 x_2 v(\gamma+\epsilon)(\gamma+\eta)}{(x_2+y_2+\epsilon)(v+\eta)} - dx_2 - \beta x_2 v$$
$$\frac{dy_2}{dt} = \beta x_2 v - a y_2$$
$$\frac{dS}{dt} = \lambda - d_{ns} S - \beta_{ns} S v$$
$$\frac{dI}{dt} = \beta_{ns} S v - a_{ns} y$$
$$\frac{dv}{dt} = k(y_1+y_2) + k_{ns} I - uv$$

In this section, it is assumed that the two immune cell clones are not in any type of direct competition with each other. The rate of helper cell proliferation only saturates with the number of helper cells belonging to the same clone, and not all specific helper cells in the system. The two clones are therefore regulated independently. The clones also do not compete through immune-mediated suppression of virus load because our model does not include helper-induced effector responses. (In many models that include effector responses, one effector clone can suppress virus load to levels that are too low to stimulate other clones, leading to competitive exclusion.) The reason for this assumption is that we seek to examine the effects of specific helper cell infection in the absence of further complicating factors. The impact of direct competition and effector responses will be explored below.

The model properties were studied largely by numerical simulations. It will be assumed that the basic reproductive ratio of the virus in the non-specific target cells alone is greater than one, ensuring the establishment of a successful infection in this system. Furthermore, we assume that each helper cell clone in isolation can become established

without dependence on initial population sizes (except zero), the conditions for which were discussed in the last section. Under these assumptions, two outcomes are observed (Fig. 1.2): (i) both helper cell clones become established. (ii) One of the helper cell clones becomes established, while the other one goes extinct. The persisting clone is the stronger one, i.e. its net rate of expansion is faster. This exclusion occurs in the absence of any competitive interactions. The reason is that the two helper cell clones are infected by a common virus population. This leads to the phenomenon of "apparent competition" (Holt, 1977), in which the stronger helper cell clone produces an amount of virus that is too high for the weaker clone to survive.

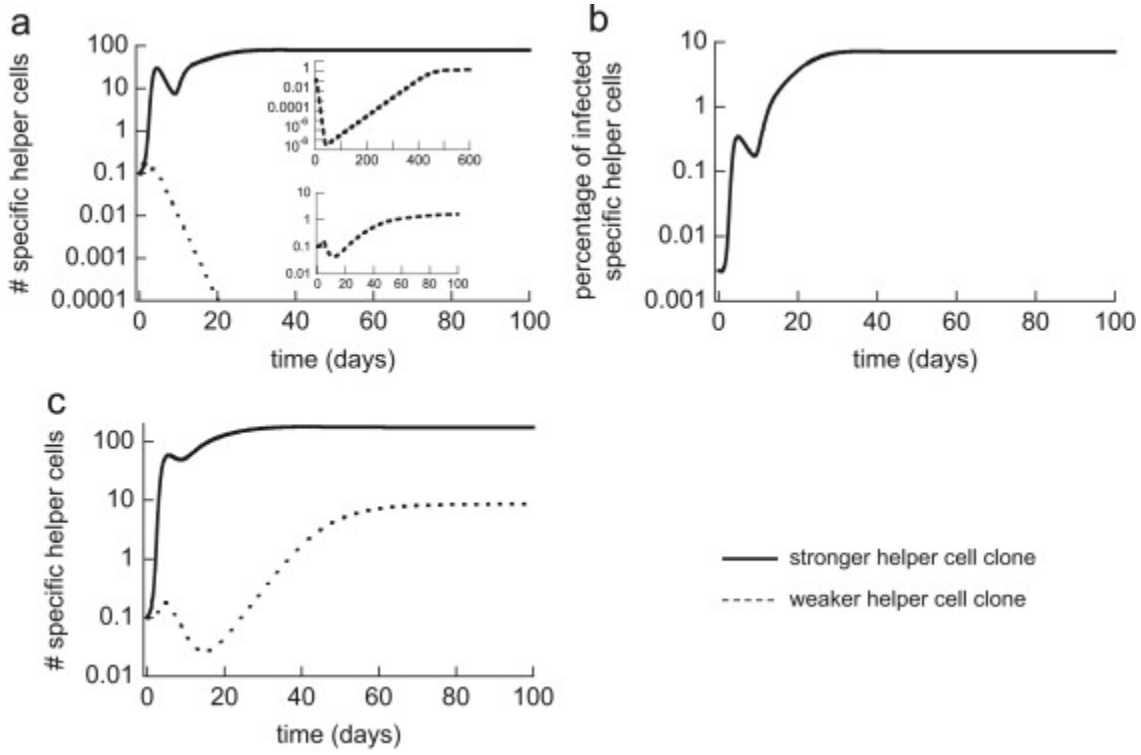

Fig. 2.2 Outcomes of model (2) assuming the presence of two virus-specific helper cell responses that are regulated independently. (a) Only one clone, the stronger one, persists. The other clone goes extinct, although it would persist in isolation (see inset). In the inset, two graphs are given. The upper graph plots the weaker helper cell response using a model without a production term for specific helper cells. Initial virus replication severely impairs the helper cell response before it settles at a steady state. The drop of this population to such low levels is likely to be unrealistic because at these low numbers, a production term can significantly influence the dynamics. In reality, the helper cell population cannot fall much below the naïve base-line levels. The lower graph displays the same simulation with a constant production term ξ=0.01 day^{-1} vol^{-1}. (b) This

graph shows the percentage of infected specific helper cells among all infected cells, corresponding to the simulation presented in part (a). (c) In this simulation, both helper cell clones coexist. For all cases, simulations can be performed for different tissue compartments or blood. In each case, the appropriate unit volume (vol) should be chosen to measure cell/viral densities. Parameters were chosen as follows: (a) β=0.015 day−1 vol; d=0.1 day−1; a=0.45 day−1; r1=0.5 day−1; r2=0.05 day−1;ε=10 vol−1; η=10 vol−1; γ=1 vol−1; k=1 day−1; u=3.33 day−1; βns=0.01 day−1 vol; λ=100 day−1 vol−1;dns=0.01 day−1; ans=0.2 day−1; kns=0.1 day−1. S(0)=λ/dns; I(0)=0.1; x1(0)=0.1; y1(0)=0; x2(0)=0.1; y2(0)=0;v(0)=1. (b) Same, except β=0.005 day−1 vol.

To make sure that these dynamics are not at odds with established quantitative parameters of HIV infection, the simulation in Fig. 1.2 was run taking into account the two most established parameter measurements (Perelson et al., 1996): an average infected cell life span of 2.2 days, and an average life-span of plasma virions of 0.3 days. The rest of the parameters, while largely uncertain, were selected such that the percentage of infected specific helper cells lies within the observed range of 1–10% (Douek et al., 2002) (Fig. 1.2). Because the non-specific target cell population encompasses several different cell types, some of which can be characterized by a relatively long life-span when infected, an overall life-span of 5 days was assigned to this population. This is necessarily arbitrary, but aims to capture the existence of both shorter lived infected T cells and the longer lived infected antigen-presenting cells in this population.

Fig. 1.3a shows how the outcome depends both on the rate of helper cell infection, β, and the death rate of infected cells, a. The base-line parameter values for this plot are taken from Fig. 1.2 and are thus within biologically realistic ranges. A lower rate of helper cell infection and a higher death rate of infected cells promote coexistence of both responses rather than exclusion. If these two parameters are influenced by immune effector responses of any kind, it can be interpreted to mean that stronger virus suppression leads to coexistence of the helper cell clones, while less efficient virus suppression leads to the exclusion outcome. The region in which exclusion of one clone is observed varies,

depending on the uncertain parameter values. In particular, the relative rates of antigen driven T cell proliferation, r_1 and r_2, play an important role, which is shown in Fig. 1.4. If the proliferation rate of the weaker clone, r_2, lies above a threshold relative to the value of r_1, coexistence is observed, otherwise, exclusion occurs. The higher the value of r_1, the higher the value of r_2 needs to be to ensure coexistence. Other parameters can also affect the outcomes, although some of them are biologically difficult to interpret, such as the saturation terms used in the model.

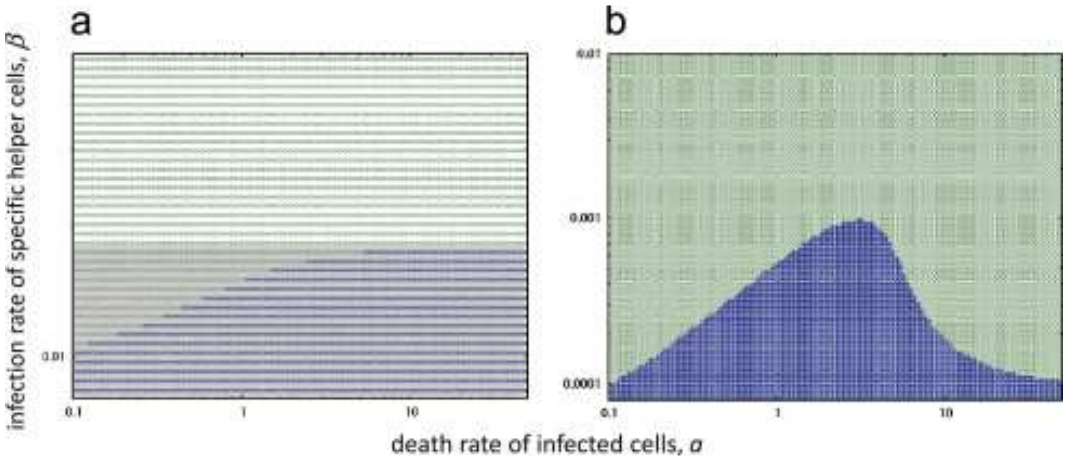

Fig. 1.3 Outcomes of model (2) depending on the death rate of infected cells, a, and the infection rate of specific helper cells, β. Blue indicates coexistence and green indicates persistence of only the stronger clone. (a) The shaded area indicates the parameter region in which the weaker clone persists in isolation. A lower death rate of infected cells and a higher infection rate of specific helper cells promotes exclusion through apparent competition. When the infection rate of specific helper cells lies above a threshold (above the shaded area), then the weaker helper cell clone never persists, even in isolation. If the infection rate of specific helper cells crosses another threshold, both helper cell populations go extinct (not shown). (b) In contrast to part (a), this plot assumes that the weaker helper cell clone cannot persist in isolation in the parameter region under consideration. In this case, a stronger helper cell clone can facilitate the maintenance of the weaker clone. This occurs for intermediate death rate of infected specific helper cells. If the infection rate of specific helper cells becomes too large this is not possible anymore because the net expansion rate of the weaker helper cell clone becomes too small. If the infection rate of specific helper cells is increased further, both helper cell clones go extinct (not shown). Base-line parameters were chosen as follows. (a) d=0.1 day^{-1}; r_1=0.5 day^{-1}; r_2=0.05 day^{-1}; ε=10 vol^{-1}; η=10 vol^{-1}; γ=1 vol^{-1}; k=1 day^{-1}; u=3.33 day^{-1}; βns= 0.01 day^{-1} vol; λ=100 day^{-1} vol^{-1}; dns=0.01 day^{-1}; ans=0.2 day^{-1}; kns=0.1 day^{-1}. (b) Same, except r1=8 day−1; r2=0.014 day−1. Initial conditions were as follows. Upon introduction of the weaker clone, the system was at the equilibrium describing persistence of the stronger clone alone (given this equilibrium was stable, as determined numerically).

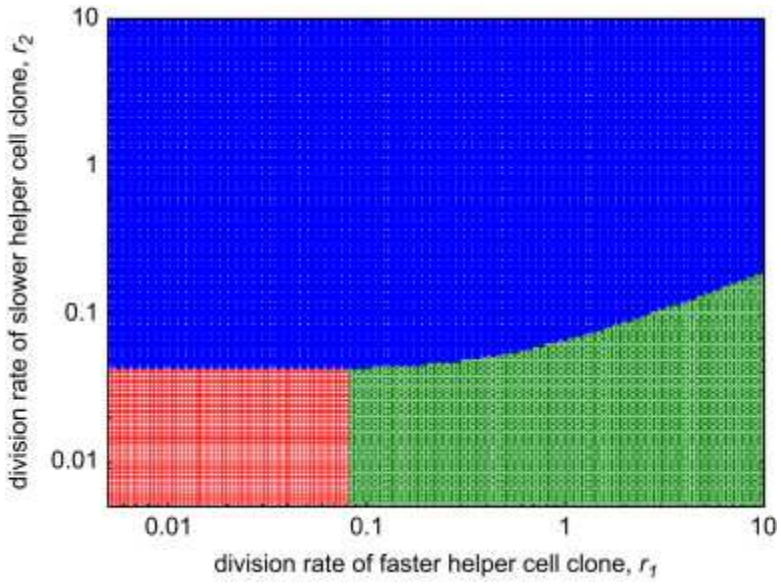

Fig. 1.4 Outcomes of model (2) depending on the antigen-induced growth rate of the stronger (r_1) and the weaker (r_2) helper cell clone. Blue indicates coexistence; green indicates persistence of only the stronger clone; red indicates extinction of both clones. Base-line parameters were chosen as follows: β=0.015 day−1 vol;d=0.1 day−1; a=0.45 day−1; ε=10 vol−1; η=10 vol−1; γ=1 vol−1; k=1 day−1; u=3.33 day−1; βns=0.01 day−1 vol; λ=100 day−1 vol−1; dns=0.01 day−1; ans=0.2 day−1; kns=0.1 day−1.

So far, we have assumed that each individual helper cell clone can establish a response in isolation. Now, we assume that only one of the helper cell clones can establish a response in isolation, and that the other one is too weak to persist. In this case, we observe a parameter region in which the presence of the stronger clone enables the weaker clone to persist as well, leading to coexistence (Fig. 1.3b, again using the base-line parameters from Fig. 1.2). The presence of the stronger clone allows additional infection to occur, and this boosts virus load to sufficient levels to also successfully stimulate the weaker clone. Hence, in this scenario, a cooperative effect occurs. This is observed for intermediate rates of infected cell death. If the death rate of infected cells is too high, not enough virus is produced by the stronger clone to maintain the weaker clone. If the death rate of infected cells is sufficiently low, too much virus is produced by the stronger clone, such that the

degree of impairment outweighs the degree of stimulation of the weaker clone. Similarly, the degree of immune impairment is too strong for the weaker clone to persist if the infection rate of specific helper cells lies above a threshold. On the other hand, if the infection rate of helper cells lies below a threshold, then the weaker clone can already persist alone without the need for the stronger clone because the degree of immune impairment is relatively weak. In general, to observe this behavior, the weaker clone must be unable to persist in isolation, and the stronger clone must provide sufficient virus for antigenic stimulation, but not too much virus to avoid significant impairment.

Effect of direct competition

So far we have assumed that each clone is regulated separately, i.e. that they do not directly compete in any way. This was done because the occurrence of competition among immune cell clones is controversial (Fryer et al., 2009 and Kastenmuller et al., 2007) and we aimed to show that even in the absence of competition, similar outcomes can be observed through indirect effects. Here, we include direct competition into the model and explore the outcomes. The model is now given by the following set of ordinary differential equations:

(Eq. 1.3)

$$\frac{dx_1}{dt} = \frac{r_1 x_1 v(\gamma+\epsilon)(\gamma+\eta)}{(x_1+y_1+x_2+y_2+\epsilon)(v+\eta)} - dx_1 - \beta x_1 v$$
$$\frac{dy_1}{dt} = \beta x_1 v - a y_1$$
$$\frac{dx_2}{dt} = \frac{r_2 x_2 v(\gamma+\epsilon)(\gamma+\eta)}{(x_1+y_1+x_2+y_2+\epsilon)(v+\eta)} - dx_2 - \beta x_2 v$$
$$\frac{dy_2}{dt} = \beta x_2 v - a y_2$$
$$\frac{dS}{dt} = \lambda - d_{ns} S - \beta_{ns} S v$$
$$\frac{dI}{dt} = \beta_{ns} S v - a_{ns} y$$
$$\frac{dv}{dt} = k(y_1+y_2) + k_{ns} I - uv$$

Direct competition is expressed in the saturation term of helper cell proliferation. In the previous model, proliferation of a particular clone only saturated when the number of cells belonging to that clone rose to higher levels. In the current model, saturation is determined by the total number of specific helper cells, belonging to either clone ($x_1+y_1+x_2+y_2$). In contrast to the previous model (2), this formulation is characterized only by one outcome: persistence of one specific helper cell clone and extinction of the other. The clone with the larger net rate of expansion persists. This is not surprising because the two clones are in direct competition with each other with no degree of niche separation.

Effector responses

So far, we have considered the dynamics of virus infection in specific helper cells in the absence of any effector responses, such as cytotoxic T lymphocyte (CTL) or B cell responses, although the helper cell responses promote the development of the effector responses, which in turn can suppress the virus population. The reason for this omission is that we wanted to see how the basic dynamics between HIV and the specific helper cells

can influence the clonal composition of the helper cell response without adding further components to the model with uncertain biological assumptions. It is thought that a broad helper cell response promotes better virus control, presumably through the induction of effector responses. The nature of the relationship between the breadth of the helper cell response and the quality and breadth of the CTL response, however, remain unknown, and conflicting experimental data have been reported (Chouquet et al., 2002, Feeney et al., 2004, Karlsson et al., 2007 and Rolland et al., 2008). In this section, we aim to show that indirect interactions can still shape the clonality of the helper cell response if a helper-dependent effector response is added to the model. As an example, we consider CTL, denoted by C. Modifying model (2) leads to the following equations:

(Eqn. 1.4)

$$\frac{dx_1}{dt} = \frac{r_1 x_1 v(\gamma+\epsilon)(\gamma+\eta)}{(x_1+y_1+\epsilon)(v+\eta)} - dx_1 - \beta x_1 v$$
$$\frac{dy_1}{dt} = \beta x_1 v - a y_1 - p y_1 C$$
$$\frac{dx_2}{dt} = \frac{r_2 x_2 v(\gamma+\epsilon)(\gamma+\eta)}{(x_2+y_2+\epsilon)(v+\eta)} - dx_2 - \beta x_2 v$$
$$\frac{dy_2}{dt} = \beta x_2 v - a y_2 - p y_2 C$$
$$\frac{dS}{dt} = \lambda - d_{ns} S - \beta_{ns} S v$$
$$\frac{dI}{dt} = \beta_{ns} S v - a_{ns} y - pIC$$
$$\frac{dv}{dt} = k(y_1+y_2) + k_{ns} I - uv$$
$$\frac{dC}{dt} = \frac{g(x_1+x_2)(y_1+y_2+I)}{qC+1} - bC$$

The rate of CTL expansion depends both on the presence of uninfected specific helper cells (x_1+x_2) and the presence of infected cells (y_1+y_2+I). Infected helper cells are assumed to be compromised. Both helper cell clones can promote CTL expansion. Helper cells are thought to activate CTL indirectly via the activation of professional antigen

presenting cells. Hence, a helper cell clone of a given specificity need not just promote one specific CTL clone, but can promote the rise of different CTL responses. In the absence of stimulation, the CTL die with a rate b. This is a phenomenological model and could be formulated in a number of different ways with a number of different assumptions. Some models of CTL dynamics assume the rate of expansion to be proportional to the number of CTL, which leads to a stronger expansion term and significantly less stable dynamics. For the current context, we have kept the model to a simple form, assuming that upon interaction with antigen and helper cells, the specific CTL population rises, presumably through an induced proliferation program, and acquires effector activity. Due to the phenomenological nature of the model, details of the CTL differentiation pathway have not been taken into account. The CTL are assumed to have both lytic and non-lytic activity. They lyse infected cells with a rate p and they inhibit the rate of virus production by infected cells with a rate q.

In this model, exclusion of one helper cell clone via indirect interactions is still observed. We thus explored the dependence of the model outcome on CTL parameters. Fig. 1.5 shows how the outcome depends on the strength of the lytic and non-lytic effector mechanisms and the rate of CTL expansion and death. The simulations are again based on the available parameter estimates used thus far. Increasing the rate of lytic or non-lytic effector activity (i.e. increasing the values of p and q, Fig. 1.5a) leads to a reduction in the amount of virus and the number of infected cells. If these rates of effector activity lie below a threshold, then apparent competition can lead to the exclusion of the weaker helper cell clone. The square in the graph indicates a sample parameter combination where we checked for biological realism. The infected specific helper cells make up about 8% of the

total infected cell population, consistent with observed ranges (Douek et al., 2002). In addition, CTL-mediated lysis contributes between 9% and 18% of total infected cell death, depending on the cell type under consideration, an order of magnitude that is consistent with previously obtained parameter estimate ranges (Asquith et al., 2006). Once the rate of effector activity crosses a threshold, exclusion does not occur anymore and the two helper cell clones coexist. This result is directly analogous to the result in Fig. 1.3a, where a reduction in the viral replication kinetics and an increase in the death rate of infected cells (parameters that are essentially altered by non-lytic and lytic CTL effector mechanisms, respectively) promoted coexistence rather than exclusion. Finally, if the rates of CTL-mediated effector activities are higher and lie above a threshold, the weaker helper cell clone again goes extinct and only the stronger clone persists. However, the mechanism is not apparent competition in this case. Strong immunity suppresses virus load (arising from all cell types) to levels that are simply too low to stimulate the weaker clone. If the rate of CTL-mediated effector activity was increased further, virus load would become too low to even stimulate the stronger helper cell clone, which, however, is not shown in Fig. 1.5a. As shown in Fig. 1.5b, similar trends are observed for the parameters that describe the rate of CTL proliferation, g, and the rate of CTL death, b. The higher the value of g and the lower the value of b, the stronger the degree of virus suppression and the lower virus load becomes. Lower degrees of virus suppression lead to exclusion of the weaker helper cell clone through apparent competition. Increasing the degree of virus suppression leads to coexistence, and a further increase in the degree of virus suppression results in levels of virus load that are too low to stimulate the weaker helper cell clone.

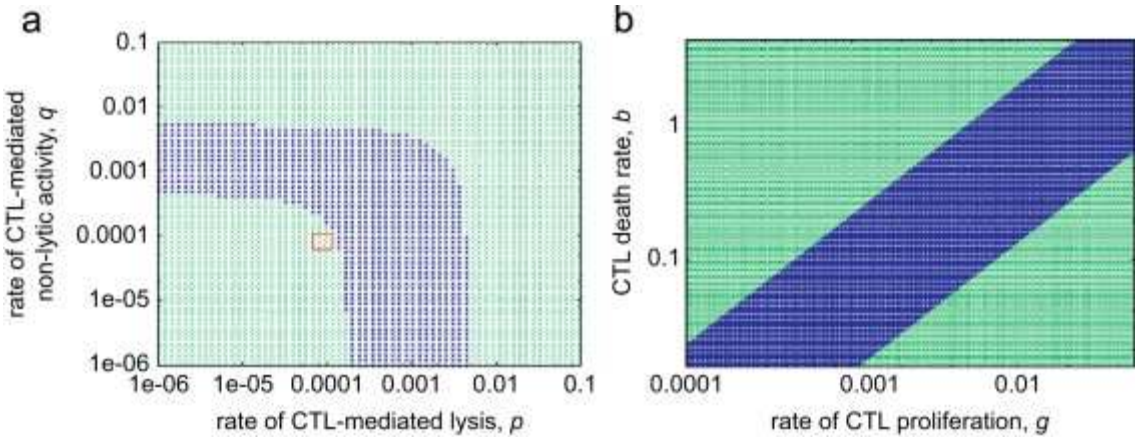

Fig. 1.5 Outcomes of model (4) depending on CTL parameters. Blue indicates coexistence; green indicates persistence of only the stronger clone. (a) Dependence on the rate of lytic, p, and non-lytic, q, effector activity. The red square indicates a parameter regime where apparent competition leads to the exclusion of the weaker helper cell clone. In this region, the specific infected helper cells make up about 8% of the total infected cell population, and CTL-mediated lysis contributes between 9% and 18% to the death rate of the infected cells. (b) Dependence on the rate of CTL proliferation, g, and the death rate of CTL, b. Base-line parameters were chosen as follows. β=0.015 day−1 vol; d=0.1 day−1; a=0.45 day−1; r1=0.5 day−1;r2=0.05 day−1; ε=10 vol−1; η=10 vol−1; γ=1 vol−1; k=1 day−1; u=3.33 day−1; βns=0.01 day−1 vol; λ=100 day−1 vol−1; dns=0.01 day−1; ans=0.2 day−1; kns=0.1 day−1; g=0.0002 day−1 vol; b=0.01 day−1; p=0.0003 day−1 vol; q=0.001 vol.

Discussion and conclusion

We have investigated the basic dynamics of HIV replication in two helper T cell clones that are specific to HIV. This extends previous work that examined HIV dynamics in a single population of specific helper T cells (Wodarz and Hamer, 2007). It is complementary to another study (Korthals Altes et al., 2003) that also examined HIV dynamics in the presence of polyclonal helper cell responses, but assumed the existence of effector responses that remove the virus population and are directly driven by the specific helper cells. They showed an array of interesting and complex behavior, including multiple steady states that are simultaneously stable. In contrast, our model considers a much

simpler scenario. The main model did not take into account helper-dependent effector responses and excluded the possibility for any competition among the helper cell clones. Nevertheless, complex dynamics were observed that included both negative and positive interactions between the helper cell clones through a shared pathogen. On the one hand, a stronger helper cell clone can exclude a weaker one through apparent competition, maintaining an amount of virus that is too high for the weaker clone to persist. On the other hand, a stronger clone can facilitate the establishment of a weaker clone by increasing the amount of antigenic stimulation to levels that are sufficient to ensure expansion of the weaker clone.

Our model set-up is likely to apply best to the initial phase of HIV infection due to the absence of helper-driven effector responses. Effector responses only arise some weeks post infection. In addition, while the exact role of help for effector cells is still debated, there is evidence that acute CTL responses develop without the need for help and that help plays a bigger role in the long-term maintenance of CTL (Borrow et al., 1996, Kaech and Ahmed, 2001, Thomsen et al., 1998, van Stipdonk et al., 2001 and van Stipdonk et al., 2003). If the dynamics described in this paper apply in the early phases of the infection, this could set the stage for the remaining disease process (Lifson et al., 1997), which is likely to be influenced by the breadth of the remaining HIV-specific helper cells (Rosenberg et al., 1997). According to the model, innate or helper-independent responses that influence the death rate of infected cells and the infection rate of the virus could play a crucial role in this respect. Both a high rate of cell killing and a low infection rate promote coexistence of the different helper cell clones, consistent with the notion that stronger virus suppression leads to broader immune responses (Harrer et al., 1996 and Rosenberg et al., 2000). Note

that we have shown through an extension of the model that the generation of helper-dependent CTL responses does not alter our main conclusions about the role of indirect interactions for determining the clonal composition of the helper cell response, so in principle, our arguments could be valid in the longer term as well. Stronger CTL-mediated reduction of viral replication kinetics and a higher CTL-mediated death rate of infected cells is predicted to promote coexistence rather than exclusion and thus a broader response. However, it is premature to speculate about the longer term dynamics because the relationship between the nature of the helper cell response, the nature of the CTL response, and the quality of virus control remain too uncertain at this stage.

Exclusion of weaker immune cell clones by stronger ones has been explored with mathematical models in the context of cytotoxic T lymphocyte (CTL) responses. Competition for antigenic stimulation has been a major mechanism by which exclusion, and thus a narrow immune response, was explained (Nowak, 1996, Nowak et al., 1995a and Nowak et al., 1995b). In such models, coexistence between different CTL clones is difficult to achieve and has been accounted for by various mechanisms. It can occur through the evolution of antigenic escape mutants that trigger immune responses directed against new epitopes (Nowak, 1996, Nowak et al., 1995a and Nowak et al., 1995b). Alternatively, persistence of multiple CTL clones can occur in a non-equilibrium situation in which the life-span of CTL precursors is sufficiently long such that extinction does not occur within a realistic time frame (Wodarz and Nowak, 2000). Finally, the complex dynamics between polyclonal helper cell responses and helper-driven CTL mentioned above can allow for the persistence of broad responses (Korthals Altes et al., 2003). The difficulty in achieving coexistence of immune cell clones in the context of direct competition is further reflected in

our model extension in which both helper cell clones can negatively impact the expansion of either clone. Survival of only one helper cell clone was the only possible outcome under this assumption. The notion that direct competition shapes the dynamics of immune responses remains controversial (Fryer et al., 2009 and Kastenmuller et al., 2007). According to our model, however, exclusion can be observed among different HIV-specific helper cell clones even in the absence of any competition, simply as a consequence of the fact that they are infected and killed by the same virus population. This certainly can be a reasonable assumption to make, since a substantial amount of mixing of cells and viruses occurs in the blood, and even within lymph nodes. In contrast to direct competition, coexistence of the helper cell clones can readily occur.

Obviously, in vivo more than two helper cell clones can arise. The principles explored here, however, would still hold, albeit in a more complex setting. Depending on the exact expansion rates of the different helper cell clones, preliminary simulations (not shown) indicate that all responses can coexist, that one response leads to the exclusion of all others under consideration, or that some of the clones persist while others go extinct. This has not been explored further because consideration of two helper cell clones is sufficient to describe the main results of this study and because further exploration would only make sense once some of the notions explored here have been shown to be relevant in experimental systems.

It is encouraging that the dynamics described here are observed for parameter combinations that are based on empirically measured values for the life-span of infected cells and the decay rate of free virus, and occur in regimes where the percentage of infected specific helper cells lies within measured bounds. On the other hand, a number of

uncertainties prevent more quantitatively exact approaches. First, other parameters in our model are unknown. In addition the same biological processes can be described mathematically in a variety of ways, which in turn could potentially influence results. Related to this, our uncertainly about the exact processes that occur during helper cell activation, and the consequently phenomenological nature of the model, provides further difficulties for parameterizing the equations and for providing quantitatively exact predictions. Finally, our model (like most models) does not take into account all aspects of HIV biology that may influence details of the dynamics and the interpretation of parameters. For example, while our model assumes virus spread through cell-free virions, recent evidence indicates that direct cell-to-cell transmission might be as important (Hubner et al., 2009). Moreover, it has to be noted that different micro-environments for HIV replication can be spatially separated. Distinct quasi-species compositions have been observed in different anatomical areas of an HIV-infected patient, and this presents a spatially complex scenario that has not been taken into account in our model (Sala et al., 1994). Such spatial considerations could potentially alter our results, which merits further investigation. Nevertheless, our modeling approach is very valuable because it highlights the key assumptions that lead to the observed dynamics and provides new insights into factors that can determine the clonal composition of helper cell responses, which might have important implications for the overall process of disease progression. A first step towards empirically testing the model predictions would be in vitro experiments that mimic the assumptions of the model and where the individual cell populations can be easily tracked over time, allowing model fitting to the data. The dynamics occurring in vivo are characterized by complications, such as spatially distinct locations where virus replication

takes place, which also renders the measurement of the appropriate populations difficult. More theoretical work will be required to analyze such more complex situations and to guide specific experiments.

References:

Antia, R., V.V. Ganusov, V.V., and Ahmed, R. 2005. The role of models in understanding CD8+ T-cell memory. Nat Rev Immunol 5:101–111

Asquith, B., C.T. Edwards, M. Lipsitch, A.R. McLean. 2006. Inefficient cytotoxic T lymphocyte-mediated killing of HIV-1-infected cells in vivo. PLoS Biol 4:90

Borrow, P. et al. 2006. CD40L-deficient mice show deficits in antiviral immunity and have an impaired memory CD8+ CTL response. J Exp Med 183:2129–2142

Chouquet, C., B. Autran, E. Gomard, J.M. Bouley, V. Calvez, C. Katlama, D. Costagliola, and Y. Riviere. 2002. Correlation between breadth of memory HIV-specific cytotoxic T cells, viral load and disease progression in HIV infection. AIDS, 16:2399–2407

Douek, D.C., L.J. Picker, and R.A. Koup. 2003. T cell dynamics in HIV-1 infection. Annu Rev Immunol 21:265–304

Douek, D.C., J.M. Brenchley, M.R. Betts, D.R. Ambrozak, B.J. Hill, Y. Okamoto, J.P. Casazza, J. Kuruppu, K. Kunstman, S. Wolinsky, Z. Grossman, M. Dybul, A. Oxenius, D.A. Price, M. Connors, and R.A. Koup. 2002. HIV preferentially infects HIV-specific CD4+ T cells. Nature, 417:95–98

El-Far, M. R. Halwani, E. Said, L. Trautmann, M. Doroudchi, L. Janbazian, S. Fonseca, J. van Grevenynghe, B. Yassine-Diab, R.P. Sekaly, and E.K. Haddad. 2008. T-cell exhaustion in HIV infection. Curr HIV/AIDS Rep 5:13–19

Feeney, M.E., Y. Tang, K.A. Roosevelt, A.J. Leslie, K. McIntosh, N. Karthas, B.D. Walker, P.J. Goulder. 2004. Immune escape precedes breakthrough human immunodeficiency virus type 1 viremia and broadening of the cytotoxic T-lymphocyte response in an HLA-B27-positive long-term-nonprogressing child. J Virol 78:8927–8930

Fryer, H.R., A. Scherer, A. Oxenius, R. Phillips, and A.R. McLean. 2009. No evidence for competition between cytotoxic T-lymphocyte responses in HIV-1 infection. Proc Biol Sci 276:4389–4397

Goulder, P.J. and B.D. Walker. 1999. The great escape—AIDS viruses and immune control. Nat Med 5:1233–1235

Goulder, P.J., R.E. Phillips, R.A. Colbert, S. McAdam, G. Ogg, M.A. Nowak, P. Giangrande, G. Luzzi, B. Morgan, A. Edwards, A.J. McMichael, and S. Rowland-Jones. 1997. Late escape from an immunodominant cytotoxic T-lymphocyte response associated with progression to AIDS. Nat Med 3:212–217

Goulder, P.J., C. Brander, Y. Tang, C. Tremblay, R.A. Colbert, M.M. Addo, E.S. Rosenberg, T. Nguyen, R. Allen, A. Trocha, M. Altfeld, S. He, M. Bunce, R. Funkhouser, S.I. Pelton, S.K. Burchett, K. McIntosh, B.T. Korber, and B.D. Walker. 2001. Evolution and transmission of stable CTL escape mutations in HIV infection. Nature 412:334–338

Harrer, T., E. Harrer, S.A. Kalams, T. Elbeik, S.I. Staprans, M.B. Feinberg, Y. Cao, D.D. Ho, T. Yilma, A.M. Caliendo, R.P. Johnson, S.P. Buchbinder, and B.D. Walker. 1996. Strong cytotoxic T cell and weak neutralizing antibody responses in a subset of persons with stable nonprogressing HIV type 1 infection. AIDS Res Hum Retroviruses 12:585–592

Ho, D.D., A.U. Neumann, A.S. Perelson, W. Chen, J.M. Leonard, and M. Markowitz. 1995. Rapid turnover of plasma virions and Cd4 lymphocytes in Hiv-1 infection. Nature 373:123–126

Holt, R.D. 1977. Predation, apparent competition and the structure of prey communities. Theor Popul Biol 12: 197–229

Hubner, W., G.P. McNerney, P. Chen, B.M. Dale, R.E. Gordon, F.Y. Chuang, X.D. Li, D.M. Asmuth, T. Huser, and B.K. Chen. 2009. Quantitative 3D video microscopy of HIV transfer across T cell virological synapses Science, 323:1743–1747

Kaech, S.M. and Ahmed R. 2001. Memory CD8+ T cell differentiation: initial antigen encounter triggers a developmental program in naive cells. Nat Immunol 2:415–422

Kalams, S.A. and B.D. Walker, B.D. 1998. The critical need for CD4 help in maintaining effective cytotoxic T lymphocyte responses J Exp Med 188:2199–2204

Karlsson, A.C., A.K. Iversen, J.M. Chapman, T. de Oliviera, G. Spotts, A.J. McMichael, M.P. Davenport, F.M. Hecht, and D.F. Nixon. 2007. Sequential broadening of CTL responses in early HIV-1 infection is associated with viral escape. PLoS One 2:225

Kastenmuller, W., G. Gasteiger, J.H. Gronau, R. Baier, R. Ljapoci, D.H. Busch, and I. Drexler. 2007. Cross-competition of CD8+ T cells shapes the immunodominance hierarchy during boost vaccination. J Exp Med 204:2187–2198

Klenerman, P., F. Lechner, M. Kantzanou, A. Ciurea, H. Hengartner, R. Zinkernagel. 2000. Viral escape and the failure of cellular immune responses. Science 289:2003

Komarova, N.L., E. Barnes, P. Klenerman, and D. Wodarz. 2003. Boosting immunity by antiviral drug therapy: a simple relationship among timing, efficacy, and success. Proc. Natl Acad Sci USA 100:1855–1860

Korthals, H., H. Altes, R.M. Ribeiro, R.J. de Boer. 2003. The race between initial T-helper expansion and virus growth upon HIV infection influences polyclonality of the response and viral set-point. Proc Biol Sci 270:1349–1358

Lifson, J.D., M.A. Nowak, S. Goldstein, J.L. Rossio, A. Kinter, G. Vasquez, T.A. Wiltrout, C. Brown, D. Schneider, L. Wahl, A.L. Lloyd, J. Williams, W.R. Elkins, A.S. Fauci, and V.M.

Hirsch. 1997. The extent of early viral replication is a critical determinant of the natural history of simian immunodeficiency virus infection. J Virol 71:9508–9514

Lifson, J.D., J.L. Rossio, R. Arnaout, L. Li, T.L. Parks, D.K. Schneider, R.F. Kiser, V.J. Coalter, G. Walsh, R.J. Imming, B. Fisher, B.M. Flynn, N. Bischofberger, M. Piatak Jr., V.M. Hirsch, M.A. Nowak, and D. Wodarz. 2000. Containment of simian immunodeficiency virus infection: cellular immune responses and protection from rechallenge following transient postinoculation antiretroviral treatment. J Virol 74:2584–2593

Mansky, L.M., and H.M. Temin. 1995. Lower in vivo mutation rate of human immunodeficiency virus type 1 than that predicted from the fidelity of purified reverse transcriptase. J Virol 69:5087–5094

McLean, A.R. and T.B.L. Kirkwood. 1990. A model of human-immunodeficiency-virus infection in T-helper cell clones. J Theor Biol 147:177–203

McMichael, A.J. and R.E. Phillips. 1997. Escape of human immunodeficiency virus from immune control. Annu Rev Immunol 15:271–296

Moir, S., T.W. Chun, and A.S. Fauci. Pathogenic mechanisms of HIV disease. 2011. Annu Rev Pathol 6:223–248

Nowak., M.A. 1990. HIV mutation-rate. Nature 347:522–522

Nowak., M.A. 1996. Immune-responses against multiple epitopes—a theory for immunodominance and antigenic variation. Semin Virol 7:83–92

Nowak, M.A., R.M. May. 2000. Virus Dynamics: Mathematical Principles of Immunology and Virology. Oxford University Press

Nowak, M.A., R.M. May, and K. Sigmund. 1995. Immune-responses against multiple epitopes. J Theor Biol 175:325–353

Nowak, M.A., R.M. May, R.E. Phillips, S. Rowlandjones, D.G. Lalloo, S. McAdam, P. Klenerman, B. Koppe, K. Sigmund, C.R.M. Bangham, and A.J. McMichael. 1995. Antigenic oscillations and shifting immunodominance in Hiv-1 infections. Nature 375:606–611

Perelson, A.S. 2002. Modelling viral and immune system dynamics. Nat Rev Immunol 2:28–36

Perelson, A.S., A.U. Neumann, M. Markowitz, J.M. Leonard, and D.D. Ho. 1996. Hiv-1 dynamics in-vivo—virion clearance rate, infected cell life-span, and viral generation time. Science 271:1582–1586

Phillips, R.E., S. Rowland-Jones, D.F. Nixon, F.M. Gotch, J.P. Edwards, A.O. Ogunlesi, J.G. Elvin, J.A. Rothbard, C.R. Bangham, C.R. Rizza, et al. 1991. Human immunodeficiency virus genetic variation that can escape cytotoxic T cell recognition. Nature 354(6353):453-9

Price, D.A., P.J. Goulder, P. Klenerman, A.K. Sewell, P.J. Easterbrook, M. Troop, C.R. Bangham, and R.E. Phillips. 1997. Positive selection of HIV-1 cytotoxic T lymphocyte escape variants during primary infection. Proc Natl Acad Sci USA 94:1890–1895

Rolland, M., D. Heckerman, W. Deng, C.M. Rousseau, H. Coovadia, K. Bishop, P.J. Goulder, B.D. Walker, C. Brander, J.I. Mullins. 2008. Broad and Gag-biased HIV-1 epitope repertoires are associated with lower viral loads. PLoS One 3:e1424

Rosenberg, E.S., and B.D. Walker. 1998. HIV type 1-specific helper T cells: a critical host defense. AIDS Res Hum Retroviruses 14:S143–S147

E.S. Rosenberg, E.S., L. LaRosa, T. Flynn, G. Robbins, and B.D. Walker. 1999. Characterization of HIV-1-specific T-helper cells in acute and chronic infection. Immunol Lett 66:89–93

E.S. Rosenberg, E.S., J.M. Billingsley, A.M. Caliendo, S.L. Boswell, P.E. Sax, S.A. Kalams, and B.D. Walker. 1997. Vigorous HIV-1-specific CD4+ T cell responses associated with control of viremia. Science, 278:1447–1450

Rosenberg, E.S., M. Altfeld, S.H. Poon, M.N. Phillips, B.M. Wilkes, R.L. Eldridge, G.K. Robbins, R.T. D'Aquila, P.J. Goulder, and B.D. Walker. 2000. Immune control of HIV-1 after early treatment of acute infection. Nature 407: 523–526

Sala, M., G. Zambruno, J.P. Vartanian, A. Marconi, U. Bertazzoni, S. Wain-Hobson. 1994. Spatial discontinuities in human immunodeficiency virus type 1 quasispecies derived from epidermal Langerhans cells of a patient with AIDS and evidence for double infection. J Virol 68:5280–5283

Simon, V. and D.D. Ho. 2003. HIV-1 dynamics in vivo: implications for therapy. Nat Rev Microbiol 1:181–190

Thomsen, A.R., A. Nansen, J.P. Christensen, S.O. Andreasen, O. Marker. 1998. CD40 ligand is pivotal to efficient control of virus replication in mice infected with lymphocytic choriomeningitis virus. J Immunol 161:4583–4590

van Stipdonk, M.J.B., E.E. Lemmens, and S.P. Schoenberger. 2001. Naive CTLs require a single brief period of antigenic stimulation for clonal expansion and differentiation. Nat Immunol 2:423–429

van Stipdonk, M.J.B., G. Hardenberg, M.S. Bijker et al., 2003. Dynamic programming of CD8+ T lymphocyte responses. Nat Immunol 4:361–365

Wei, X.P., S.K. Gosh, M.E. Taylor et al., 1995. Viral dynamics in human-immunodeficiency-virus type-1 infection. Nature 373(6510):117–122

Wodarz, D. 2006. Killer Cell Dynamics: Mathematical and Computational Approaches to Immunology. Springer, New York

Wodarz, D. and Nowak, M.A. 1999. Specific therapy regimes could lead to long-term control of HIV. Proc Natl Acad Sci USA 96:14464–14469

Wodarz, D. and Nowak, M.A. 2000. CD8 memory, immunodominance and antigenic escape. Eur J Immunol 30: 2704–2712

Wodarz, D. and Jansen, V.A.A. 2001. The role of T cell help for anti-viral CTL responses. J Theor Biol 211:419–432

Wodarz, D. and Hamer, H. 2007. Infection dynamics in HIV-specific CD4 T cells: does a CD4 T cell boost benefit the host or the virus? Math Biosci 209:14–29

Wodarz, D., Arnaout, R.A., Nowak, M.A., and Lifson, J.D. 2000. Transient antiretroviral treatment during acute simian immunodeficiency virus infection facilitates long-term control of the virus. Philos Trans R Soc London B Biol Sci 355:1021–1029

Younes, S.A., L. Trautmann, B. Yassine-Diab, et al. 2007. The duration of exposure to HIV modulates the breadth and the magnitude of HIV-specific memory CD4+ T cells. J. Immunol 178:788–797

Chapter 2: Tissue architecture, feedback regulation, and resilience to viral infection

Abstract

Tissue homeostasis is one of the central requirements for the existence of multicellular organisms, and is maintained by complex feedback regulatory processes. Homeostasis can be disturbed by diseases such as viruses and tumors. Here, we use mathematical models to investigate how tissue architecture influences the ability to maintain tissue homeostasis during viral infections. In particular, two different tissue designs are considered. In the first scenario, stem cells secrete negative feedback factors that influence the balance between stem cell self-renewal and differentiation. In the second scenario, those feedback factors are not produced by stem cells but by differentiated cells. The model shows a tradeoff. If feedback factors are produced by stem cells, then a viral infection will lead to a significant reduction in the number of differentiated cells leading to tissue pathology, but the number of stem cells is not affected at equilibrium. In contrast, if the feedback factors are produced by differentiated cells, a viral infection never reduces the number of tissue cells at equilibrium because the feedback mechanism compensates for virus-induced cells death. The number of stem cells, however, becomes elevated, which could increase the chance of these stem cells to accumulate mutations that can drive cancer. Interestingly, if the virus interferes with feedback factor production by cells, uncontrolled growth can occur in the presence of the virus even in the absence of genetic lesions in cells. Hence, the optimal design would be to produce feedback factors by both

stem and differentiated cells in quantities that strike a balance between protecting against tissue destruction and stem cell elevation during infection.

Introduction

The functioning of multicellular organisms requires tight regulation of cellular behavior such that the number of tissue cells is maintained at constant levels. Human adult tissue is thought to be maintained by tissue stem cells that have self-renewal capacity. The tissue stem cells differentiate into transit amplifying cells that are capable of a limited number of divisions, and further differentiation results in terminally differentiated cells that cannot divide anymore (Crosnier et al., 2006). Terminally differentiated cells perform their function that is required for the tissue, and die after a certain period of time. Homeostasis is thought to be achieved by various negative feedback loops (Daluiski et al., 2001, Elgjo and Reichelt, 2004, Lander et al., 2009, McPherron et al., 1997, Tzeng et al., 2011, Wu et al., 2003 and Yamasaki et al., 2003). An important process that is subject to regulation is the decision for stem cells to self-renew upon division (giving rise to two daughter stem cells), or to differentiate, thus giving rise to two daughter cells that are on the path to terminal differentiation. As the number of cells grows, feedback factors have been shown to block self-renewal and promote differentiation instead, which limits tissue size through the eventual death of terminally differentiated cells. Other feedback factors down-regulate the rate of cell division as the number of cells grows, thus also preventing excessive growth. Such feedback loops have been observed in a variety of tissues (Daluiski et al., 2001, Elgjo and Reichelt, 2004, Lander et al., 2009, McPherron et al., 1997, Tzeng et

al., 2011, Wu et al., 2003 and Yamasaki et al., 2003) and many feedback factors have been found to belong to the transforming growth factor β (TGF-β) superfamily. For example, GDF11 is produced by neuronal cells in the mouse olfactory epithelium and provides feedback to inhibit the production of neurons. Lack of GDF11 leads to elevated production of neurons (Lander et al., 2009).

Tissue homeostasis can be disturbed by diseases. The development of tumors obviously leads to uncontrolled cell growth. Viral infection can lead to the depletion of tissue cells and compromised tissue function. There is also an interplay between viral infections and the development of tumors, with several viruses thought to contribute to tumor initiation (Butel, 2000 and Zur Hausen, 2009). Because viral infections can destroy tissue cells, they thereby influence the feedback dynamics of the tissue, for example by reducing the level of feedback inhibition and thus inducing altered levels of cell proliferation and differentiation. In this paper we use mathematical models to study the consequences of viral infections for the dynamics of feedback regulation in otherwise healthy tissue. In particular, we ask how the design of regulatory circuits affects the protection against pathology. The models suggest the presence of an important tradeoff: if the regulatory mechanisms are designed to provide maximal protection against virus-induced tissue destruction, this can lead to increased levels of stem cell proliferation, which can promote the development of cancers. Interestingly, it is shown that in this case, viral interference with feedback factor production can lead to uncontrolled cellular proliferation even in the absence of induced genetic lesions in cells. In contrast, if tissue is designed to minimize the impact of the infection on stem cell proliferation, then virus-induced tissue

destruction is maximized. Hence, evolution is likely to favor a tissue design that optimizes this tradeoff.

Results

A model will be considered that includes two basic populations: (i) cells with self-renewal capacity, which includes both tissue stem cells and transit amplifying cells. For simplicity, this population will be collectively referred to as "stem cells", and is denoted by S. (ii) Terminally differentiated cells that cannot divide anymore, denoted by D. It is based on previous models (Lander et al., 2009, Lo et al., 2009 and Rodriguez-Brenes et al., 2011) and given by the following set of ordinary differential equations that describe the time evolution of these cell populations.

(Eqn. 2.1)

$$\frac{dS}{dt} = r'Sp' - (1-p')r'S$$
$$\frac{dD}{dt} = 2(1-p')r'S - aD$$

This represents a minimally parameterized model to describe tissue dynamics, which allows us to obtain analytical insights. Stem cells divide with a rate r'. With a probability p', division results in two daughter stem cells (self-renewal). With a probability $1 - p'$, division results in two differentiated cells. Differentiated cells die with a rate a. The primes in the notation mean that these parameters can be influenced by negative feedback. Feedback factors can either be produced by stem cells or by differentiated cells. In the context of differentiation, this is expressed as $p' = p/(n_1 S + n_2 D + 1)$. Thus, the basic probability of self-renewal is given by p, and the parameters n_1 and n_2 describe the relative

strength of feedback factors produced by stem and differentiated cells, respectively. Feedback on the rate of cell division is expressed by $r' = r/(m_1 S + m_2 D + 1)$. The parameter r describes the intrinsic rate of cell division, and the relative strength of feedback factors produced by stem and differentiated cells is given by m_1 and m_2, respectively.

Next, we introduce a viral infection into this model, assuming that the virus can only infect differentiated cells and not the stem cells. Denoting infected differentiated cells by *I,* this is formulated as follows according to standard virus dynamics equations.

(Eqn. 2.2)

$$\frac{dS}{dt} = r'Sp' - (1-p')r'S$$
$$\frac{dD}{dt} = 2(1-p')r'S - aD - bDI$$
$$\frac{dI}{dt} = bDI - a_d I$$

The infection is modeled based on established virus dynamics formulations (Nowak and May, 2000 and Perelson, 2002). Upon contact with uninfected differentiated cells, infection occurs with a rate b. Infected cells die with a rate a_d. Free virus particles are not explicitly taken into account but are assumed to be in a quasi-steady state. This is a well justified assumption in the field (Nowak and May, 2000) because the turnover of free virus is much faster than that of infected cells. In the presence of the virus infection, two types of differentiated cells exist (uninfected and infected), and both can potentially secrete feedback factors. Infected cells can maximally produce the same amount of feedback factors as uninfected cells, but may produce less due to viral impairment. Thus, the self-renewal feedback is now given by: $p' = p/(n_1 S + n_2 D + f n_2 I + 1)$, where $f \leq 1$. Similarly, the division feedback is given by $r' = r/(m_1 S + m_2 D + g m_2 I + 1)$, where $g \leq 1$.

We will start by analyzing a scenario where there is only feedback on self-renewal/differentiation (p'). No feedback on the rate of cell division will be assumed to exist for now. Feedback on self-renewal is the most important feedback loop that enables the existence of a stable equilibrium in this system (Lander et al., 2009 and Lo et al., 2009), and this simplification helps us obtain some key results. Subsequently, feedback on the rate of cell division is introduced and examined.

Feedback on self-renewal only

This section considers the scenario where there is feedback on self-renewal only, and the rate of cell division is simply given by the parameter r ($m_1=m_2=0$). The following outcomes are observed. Persistence of the tissue requires that $p>0.5$. In this case the system can converge to two different equilibria depending on the parameter values. If the infection is not established, the following equilibrium is observed:

$$S^{(0)}=\frac{a(2p-1)}{n_2 r+an_1}$$
$$D^{(0)}=\frac{r(2p-1)}{n_2 r+an_1}$$
$$I^{(0)}=0$$

If the virus does establish an infection, the dynamics converge to the following steady state:

$$S^{(1)}=\frac{a_d[b(2p-1)-n_2(a_d-fa)]}{b(rfn_2+a_d n_1)}$$
$$D^{(1)}=\frac{a_d}{b}$$
$$I^{(1)}=\frac{rb(2p-1)-a_d(rn_2+an_1)}{b(rfn_2+a_d n_1)}$$

Successful infection is established if the basic reproductive ratio of the virus (Anderson and May, 1991 and Nowak and May, 2000) is greater than one, given by $R_0=bD^{(0)}/a_d$.

We are interested in the effect of the infection on tissue homeostasis. Therefore, we compare the number of stem cells and differentiated cells in the presence of the infection with the number in the absence of the infection at equilibrium, expressed as ratios $S_{frac}=S^{(1)}/S^{(0)}$ and $D_{frac}=(D^{(1)}+I^{(1)})/D^{(0)}$. Let us first examine the dependence of these ratios on the viral replication rate, *b* (Fig. 2.1). We consider the effect of infection in the context of two different tissue designs. First we assume that feedback factors are only produced by stem cells and not by differentiated cells ($n_1>0$; $n_2=0$). Fig. 1a shows that in this case, the fraction of stem cells during infection, S_{frac}, is independent of the viral replication rate, *b*. The fraction of differentiated cells, D_{frac}, declines with *b* towards an asymptote because a faster replicating virus leads to a higher degree of cell depletion (Fig. 2.1a). If the basic reproductive ratio of the virus, R_0, is around its threshold value of one, there is a strong dependence. But if $R_0 \gg 1$, the dependence is weak while converging to the asymptote. Now, the opposite scenario is explored where all feedback factors are produced by differentiated cells and none by stem cells ($n_1=0$; $n_2>0$). The fraction of stem cells during infection, Sfrac, increases asymptotically with *b* (Fig. 2.1b). The reason is that a faster replicating virus kills more differentiated cells, which triggers the feedback mechanism to compensate for this, achieved through an elevation of the stem cell compartment. This dependence is again strong for R_0 around one, and becomes weak for $R_0 \gg 1$. Because of the feedback induced compensation for the death of differentiated cells, this population does not depend on the viral replication rate in this case (Fig. 2.1b).

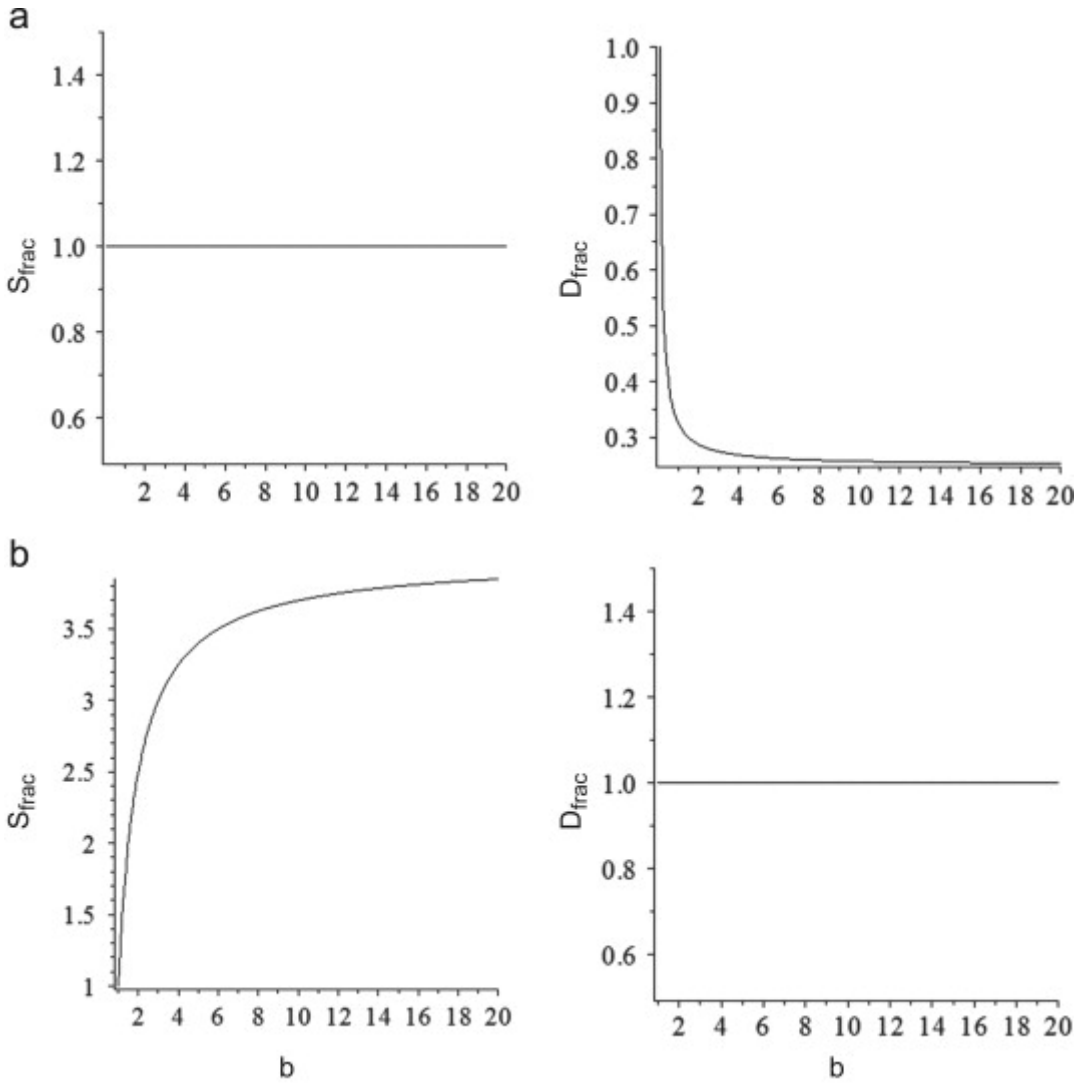

Fig. 2.1 Dependence of the measures S_{frac} and D_{frac} on the replication rate of the virus, b, according to model (2). (a) Scenario where we assume n_1=1 and n_2=0. (b) Scenario n_1=0 and n_2=1. Other parameters were chosen as follows. p=0.6, r=0.5; a=0.05; a_2=0.2; m_1=m_2=0; f=1.

Fig. 2.1 shows some interesting differences between the tissue designs. To explore this further, we make a simplification. Because the fractions S_{frac} and D_{frac} do not strongly depend on the viral replication rate b for R_0»1, we will consider these fractions at the limit b→∞, i.e. $S_{frac}^{b\to\infty}$ and $D_{frac}^{b\to\infty}$. The expressions are given by

(Eqn. 2.3)

$$S_{frac}^{b\to\infty}=\frac{a_d(n_2\,r+an_1)}{(rfn_2+a_d\,n_1)a},\ D_{frac}^{b\to\infty}=\frac{n_2\,r+an_1}{r\,fn_2+a_d\,n_1}.$$

Let us now investigate the properties of the two tissue designs in more detail. If feedback factors are only produced by stem cells ($n_1>0$; $n_2=0$), the expressions simplify as follows.

$$S_{frac}^{b\to\infty} = 1$$
$$D_{frac}^{b\to\infty} = \frac{a}{a_d}$$

That is, the presence of infection does not alter the number of stem cells, but it lowers the total number of differentiated cells. This is also shown without the simplification $b\to\infty$ in Fig. 2.2a. Since many tumors are thought to arise by mutations in stem cells, a lack of increase of this population means that the infection is not likely to increase the risk of carcinogenesis. Tissue size is compromised, however, and the degree of reduction in the number of differentiated cells is given by the virus-induced death rate of infected cells, a_d, compared to the death rate of uninfected cells, a. Therefore, if the virus kills the cells relatively fast (cytopathic virus), the degree of pathology is predicted to be large.

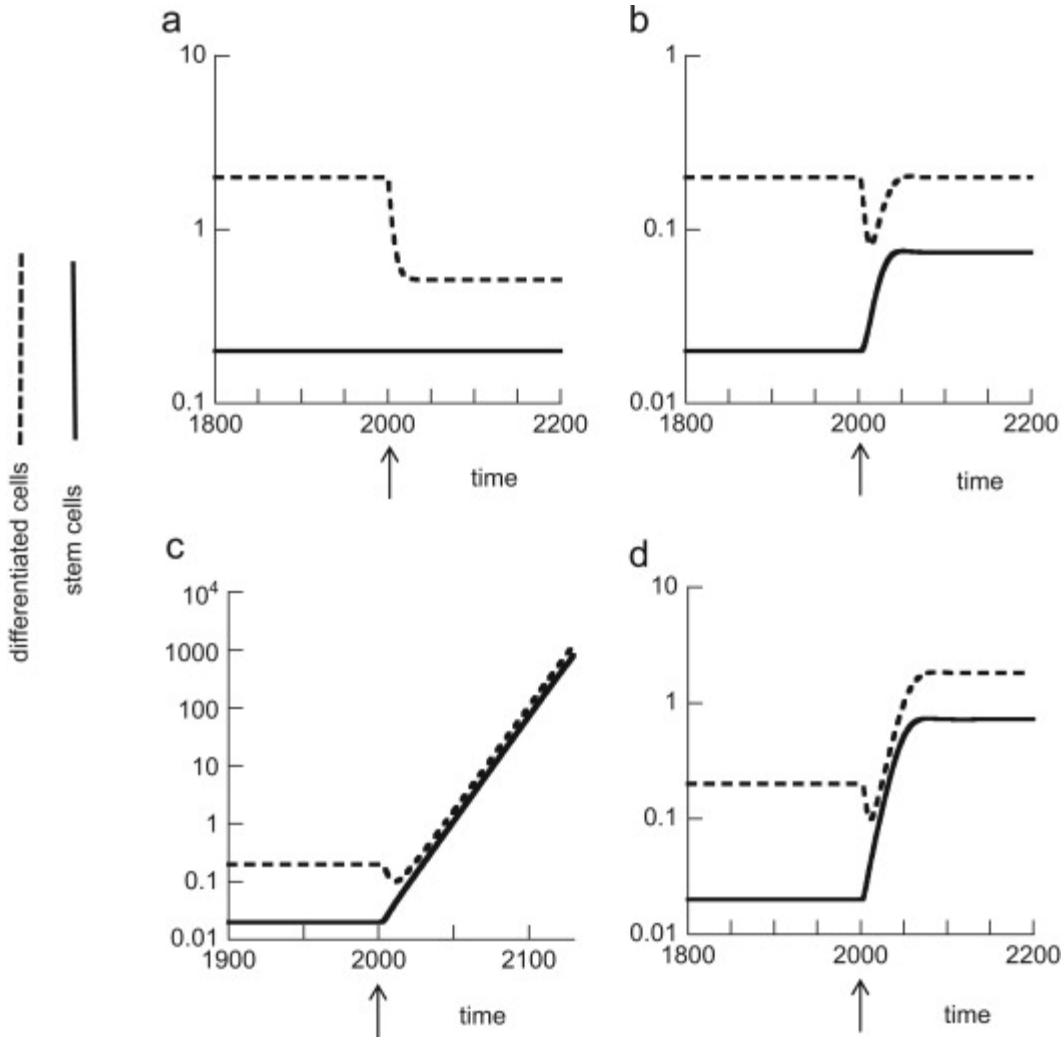

Fig. 2.2 Tissue architecture and resilience to infection, according to model (2). Arrow indicates infection. (a) Scenario where we assume n_1=1 and n_2=0 as well as f=1. Stem cell numbers remain steady during infection but differentiated cells decline. (b) Scenario where we assume n_1=0 and n_2=1 as well as f=1. Infection does not alter the equilibrium number of differentiated cells, but the number of stem cells grows. For n_1=*0* and n_2>*0*, uncontrolled tissue growth is observed if f<1, shown in (c) f=0 and (d) f=0.1. Other parameters were chosen as follows. b=10; p=0.6, r=0.5; a=0.05; a2=0.2; m_1=m_2=0.

In the opposite case, where only differentiated cells produce feedback factors (n_1=0; n_2>0), the expressions or $S_{frac}^{b\to\infty}$ and $D_{frac}^{b\to\infty}$ simplify as follows.

(Eqn. 2.4)

$$S_{frac}^{b\to\infty}=\frac{a_d}{fa}$$

$$D_{frac}^{b\to\infty}=\frac{1}{f}$$

Let us first assume that the virus does not impair feedback production by infected cells, i.e. f=1. Now, we find that the virus infection does not reduce the number of tissue cells, thus leading to absence of virus-induced pathology. The number of differentiated cells remains identical compared to the level in the absence of the infection. Note that this result is independent of the rate of virus-induced cell death and also applies to cytopathic viruses. Virus-induced cell death is compensated for by feedback modulation. The number of stem cells, however, is increased by the infection, proportional to the degree of viral cytopathicity, a_d. The higher the death rate of infected relative to uninfected cells, the larger the elevation of the stem cell population. These trends are also shown in the absence of the simplification $b \to \infty$ in Fig 2.2b. A higher number of stem cells means more stem cell divisions, which increases the chances of mutations. This in turn increases the chances of cancer initiation. Next, assume that the virus impairs the production of feedback factors in infected cells, i.e.f<1. In the extreme case, f=0, we find that both the differentiated and the stem cell populations increase towards infinity (Fig 2.2c). In other words, unbounded proliferation of stem cells is observed, which would correspond to a tumor. Interestingly, unbounded growth does not necessarily rely on any genetic alteration in the cells. If viral replication compromises the function of differentiated cells, resulting in the lack of feedback factor production, the tissue becomes dysregulated, leading to cancerous growth. If feedback factor production is not completely abolished but reduced (0<f<1), the cell populations rise towards a new steady state (Fig 2.2d), the level of which is determined by the value of f. While growth is not unbounded anymore, this can also be considered cancerous growth. In fact, many cancers are characterized by growth periods, followed by periods of stasis.

In the above analysis it was assumed that virus infection can reduce the level of feedback factor production (f<1). This is a reasonable assumption because viruses can compromise cellular function in a variety of ways. Theoretically, it is also possible that the presence of the virus enhances feedback factor production (f >1), e.g. by up-regulating gene expression. As is clear from the above expressions for $S_{frac}^{b\to\infty}$ and $D_{frac}^{b\to\infty}$, this would reduce both the number of stem and differentiated cells, thus promoting tissue pathology.

In summary, there is a tradeoff in the design of regulatory circuits in the context of viral infections. If feedback factors are produced mostly by stem cells, then stem cell homeostasis remains unaltered during viral infections, but maximal virus-induced tissue destruction is observed. In contrast, if feedback factors are produced mostly by differentiated cells, then tissue destruction will not be observed, but there is a high risk of developing cancer due to elevated stem cell replication. Therefore, the best design, i.e. the one most likely favored by evolution, will be a balance of feedback factor production by stem and differentiated cells that optimizes this tradeoff. It is currently not possible to calculate this optimal tradeoff. As can be seen from the full expressions for or $S_{frac}^{b\to\infty}$ and $D_{frac}^{b\to\infty}$ (Eqn. 2.3), a change in either parameter results in an equal change in $S_{frac}^{b\to\infty}$ and $D_{frac}^{b\to\infty}$. For example, a 2-fold increase in n_1 leads to the same fold reduction in the values of $S_{frac}^{b\to\infty}$ and $D_{frac}^{b\to\infty}$. That is, the number of stem cells during infection is reduced towards its pre-infection levels (thus reducing risk of carcinogenesis), and the number of differentiated cells is reduced below its pre-infection level by the same amount, thus increasing the degree of pathology.

The uncertain part is how to interpret this. Although a given change in the degree of feedback inhibition changes the number of stem cells by as much as it changes the number of differentiated cells, it is unclear how this change in homeostasis relates to disease development. For example it is possible that a 2-fold reduction in the number of stem cells only marginally reduces the chances to generate carcinogenic mutations, but that a 2-fold reduction in the number of differentiated tissue cells kills the organism. These types of considerations will determine the optimal balance between n_1 and n_2, and hence this is currently not possible to calculate.

Feedback on self-renewal and cell division rate

Here, we consider the additional negative feedback on the rate of cell division, i.e. $m_1>0$ and $m_2>0$. Feedback factors can again be produced either by stem cells (m_1) or differentiated cells (m_2). This model is studied numerically because equilibrium expressions are very complex and not insightful and hence not written down here. The results described in the previous section still hold in this more complex situation. If the viral infection leads to increased cell growth, the growth rate is slower in the presence of this additional feedback (Fig 2.3). This makes sense because the feedback slows down the rate of cell division. Such a slow growth pattern in the presence of feedback on cell division has recently been described (Rodriguez-Brenes et al., 2011).

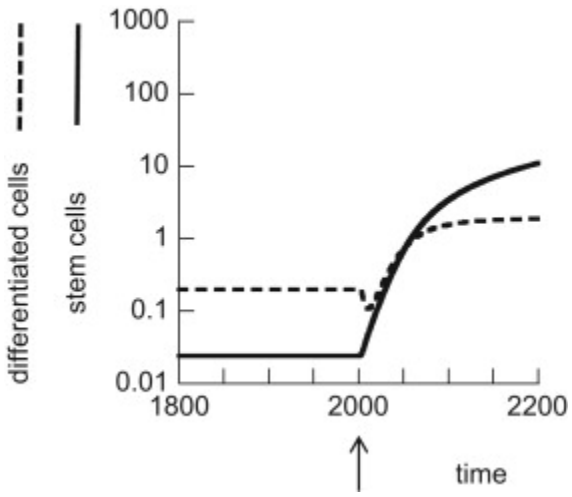

Fig. 2.3 Uncontrolled growth in the context of negative feedback on the cell division rate, according to model (2). Arrow indicates infection. Parameters were chosen as follows. b=10; n1=0; n2=1. p=0.6, r=0.5; a=0.05; a_2=0.2; m1=m2=1; f=0; g=0.

Infection of stem cells

So far, it was assumed that only differentiated cells become infected. Here it will be assumed that stem cells can also become infected. This has been documented to occur in retroviruses and other viruses (Banerjee et al., 2010), although typically the virus does not tend to be very active in stem cells but can be transmitted by cell division. The following model describes stem cell infection.

(Eqn. 2.6)

$$\frac{dS}{dt} = r'Sp' - (1-p')r'S - b_S S(I_d + \eta I_s)$$
$$\frac{dD}{dt} = 2(1-p')r'S - aD - b_d D(I_d + \eta I_S)$$
$$\frac{dI_s}{dt} = b_s S(I_d + \eta I_S) - a_s I_s + rI_s p - (1-p')rI_s$$
$$\frac{dI_d}{dt} = b_d D(I_d + \eta I_S) - a_d I_d + 2(1-p')rI_s$$

Now there are two infected cell populations instead of one. The infected differentiated cells are denoted by I_d, while the infected stem cells are denoted by I_s. Both populations die with rate a_d and a_s, respectively. Infection of differentiated and stem cells occurs with a rate b_d and b_s, respectively, and the rate of virus production is assumed to be different in stem and differentiated cells, expressed by the factor η. We will only consider feedback on differentiation, described by $p'=p/(n_1S+f_sn_1I_s+n_2D+f_dn_2I_d+1)$. The difference compared to model (2) is that virus infection can not only inhibit feedback production in differentiated cells but also in stem cells, described by parameters f_d and f_s, respectively. This model gives rise to equilibrium expressions that are too complex to obtain, so the model is explored numerically.

In model (2), which only took account of differentiated cell infection, there were two basic outcomes. Either the infection was not established or the infection was established in which case the dynamics converged to the internal equilibrium. With stem cell infection, there are two internal equilibria (Fig 2.4). In one case, all populations persist, as before (Fig 2.4a). In the alternative case, the population of uninfected stem cells goes extinct and only infected stem cells persist (Fig 2.4b). Consequently, the number of uninfected differentiated cells also goes extinct. Extinction of uninfected cells occurs because of indirect competition (Holt, 1977). Both infected and uninfected stem cells proliferate, and their population sizes are regulated by the production of negative feedback signals. While proliferation is assumed to occur with the same rate in both populations, the infected cell population gains at the expense of the uninfected cell population due to the process of infection. Hence, the infected cells can grow to higher levels and produce more negative feedback signals than

the uninfected cell population, which is consequently driven to extinction through feedback-induced terminal differentiation and death.

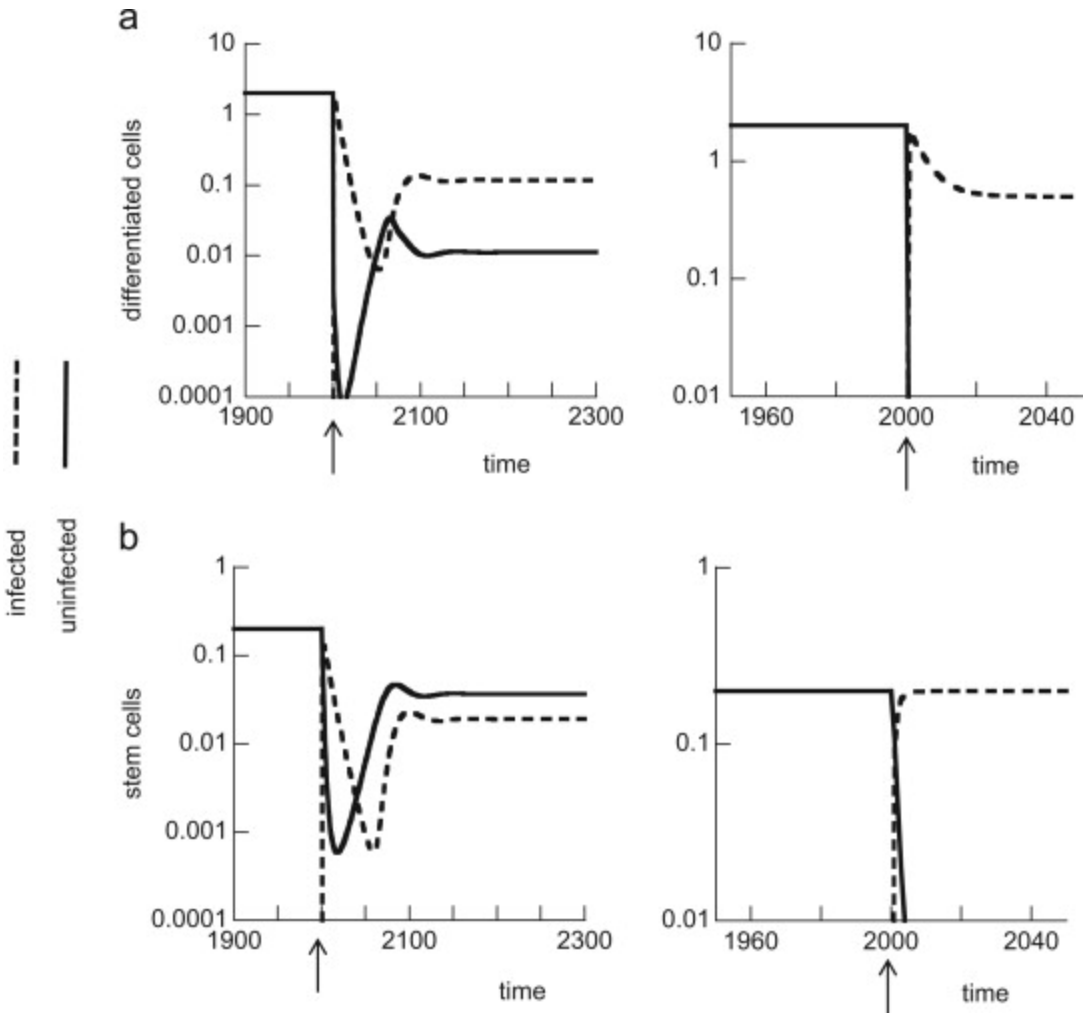

Fig. 2.4 Two different virus persistence equilibria in the stem cell infection model (6), illustrated for case wheren_1=1 and n_2=0. Arrows indicate infection. (a) Either both uninfected and infected cells persist or (b) only infected cells persist and the uninfected cells go extinct. Parameters were chosen as follows. b_d=10;b_s=0.5; p=0.6, r=0.5; a=0.05; a_d=0.2; m_1=m_2=0; fs=f_d=1, η=1. (a) a_s=0.2 (b) a_s=0.

Fig. 2.5 explores numerically under which conditions these two outcomes are achieved. Two parameters were varied: the rate of stem cell infection, b_s, and the rate of infected stem cell death, as. Simulations were run until the population of uninfected stem cells either reached equilibrium (persistence) or declined to extinction. The outcome was

coded by different colors and symbols, with blue (x) indicating persistence and red (+) extinction. In many virus infections, it is thought that there is a correlation between the rate of virus production and the death rate of infected cells. Hence, in Fig. 2.5, we assumed that the parameters η and as are positively correlated, i.e. a higher rate of virus production leads to a higher rate of cell death in the infected stem cells. As seen in Fig. 2.5, a higher rate of stem cell infection (higher b_s) and a lower death rate of infected cells (lower a_s) promote the extinction of uninfected stem cells. As mentioned above, stem cell infecting viruses tend to be characterized by a relatively low replicative activity in the stem cells, indicating a low degree of cell killing. Hence, it is likely that such viruses will lead to the infection of the whole stem cell population (Fig. 2.5).

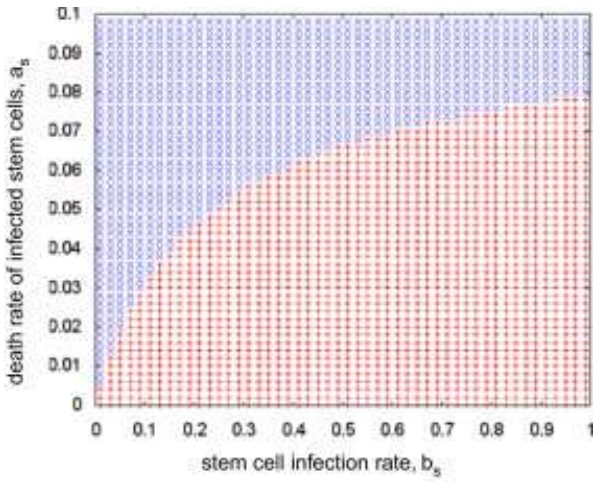

Fig. 2.5 Whether uninfected stem cells persist or not in the stem cell infection model (6) depends on parameters, which is explored numerically. The rate of stem cell infection, b_s, and the death rate of infected stem cells, a_s, was varied and the outcome is coded by different colors and symbols. Persistence of uninfected stem cells is shown in blue (*x*), and extinction in red (+). Parameters were chosen as follows. b_d=10; p=0.6, r=0.5; a=0.05; a_d=0.2; m_1=m_2=0; f_s=f_d=1, η=a_s.

In order to examine the impact of the infection on tissue homeostasis, let us therefore first assume that the virus is weakly cytopathic in stem cells (i.e. small value of a_s) and that hence all stem cells are infected. Now the expression for S_{frac} and D_{frac} do not depend on the

infection rates anymore, because all susceptible cells are infected and virus spread is driven only by the division of infected cells. For the case $n_1=0$ and $n_2>0$, we obtain:

$$S_{frac} = \frac{ra_d[r(2q-1)-a_s]}{f_d a_d (2q-1)(r^2-a_s^2)}$$
$$D_{frac} = \frac{r(2q-1)-a_s}{f_d(2q-1)(r+a_s)}.$$

If the value of *as* is small relative to *r*, this converges to

$$S_{frac} = \frac{a_d}{f_d a}$$
$$D_{frac} = \frac{1}{f_d},$$

which is identical to expression (5) above. For the case $n_1>0$ and $n_2=0$, we obtain:

$$S_{frac} = \frac{r(2q-1)-a_s}{f_s(r+a_s)(2q-1)}$$
$$D_{frac} = \frac{a[r^2(2q-1)+a_s(a_s-2rq)]}{f_s a_d r(r+a_s)(2q-1)}.$$

If the value of a_s is small relative to *r*, this converges to

$$S_{frac} = \frac{1}{f_s}$$
$$D_{frac} = \frac{a}{f_s a_d}.$$

This is similar to expression (4) above, with the addition that feedback signal impairment in stem cells, *fs*, now influences the outcome of infection. Thus, if the virus impairs feedback factor production in stem cells, uncontrolled cellular growth is possible in this scenario as well, brought about by compromised feedback regulation in the absence of genetic transformation of cells.

Therefore, the basic conclusions obtained for the model without stem cell infection hold. The only difference is that impairment of feedback factor production in stem cells can also contribute to uncontrolled cancerous growth. Note, however, that viral persistence in

stem cells can further have other effects not accounted for in the model, such as the genetic transformation of cells, which can again promote the initiation of cancer in the long term.

In contrast, if the value of a_s is larger and consequently both uninfected and infected stem cells persist, the situation is more complex. In principle, the conclusions reached from model (2) hold (Fig 2.6) but the population sizes of both the stem cells and the differentiated cells are lower, leading to tissue pathology due to a stem cell killing. Thus, in the cases when population levels were predicted to remain constant in the face of infection in model (2), infection can now reduce them due to virus-induced stem cell death (Fig 2.6) Since in most cases of stem cell infection the virus does not show significant replicative activity in stem cells, this scenario is not further explored.

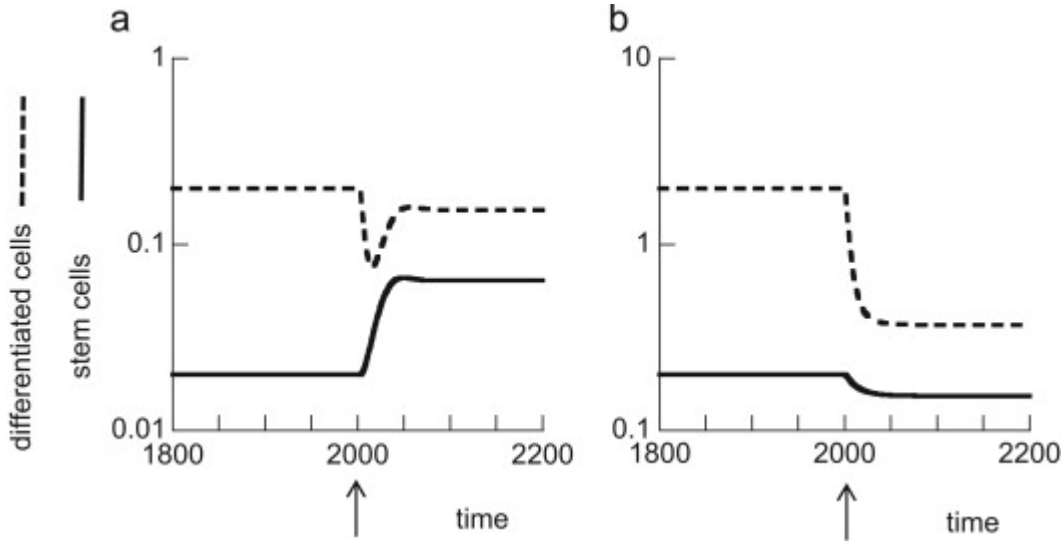

Fig. 2.6 Effect of the virus in the stem cell infection model (6) in the parameter regime where uninfected and infected cells coexist. (a) n1=0; n2=1 and (b) n1=1; n2=0. Basic properties shown in Fig. 2 still hold, but both the population of stem and differentiated cells can be lower due to virus-induced stem cell killing. Arrows indicate infection. The remaining parameters were chosen as follows. bd=10; bs=0.5; p=0.6, r=0.5; a=0.05; a_d=0.2; a_s=0.02; m_1=m_2=0; f_s=f_d=1, η=1.

To conclude, this section showed that taking into account stem cell infection does not lead to significant changes to our results derived from the model without stem cell

infection. In the biologically realistic scenario where the virus does not kill the stem cells with significant rates, the whole tissue stem cell population becomes infected, and the results regarding tissue homeostasis remain largely unchanged. In the less realistic scenario when the virus kills stem cells with relatively large rates, additional tissue pathology can occur due to stem cell death. Interestingly, this suggests that at least in the short term, the infection is less detrimental to the host if the entire stem cell population becomes infected, although the long-term cost can be a higher chance of genetic transformation and hence the development of cancer.

Discussion and conclusion

We investigated how the design of feedback control influences the tissue response to infection. An important difference was observed depending on whether the feedback factors are secreted from the differentiated cells or the stem cells. Secretion from stem cells only ensures that during a viral infection, the stem cell population remains constant, thus minimizing the risk of mutagenesis which could come about from increased levels of cell division. This, however, comes at the cost of maximally possible virus-induced tissue pathology. On the other hand, if feedback factors are secreted from differentiated cells only, then virus-induced tissue pathology is entirely absent because any cell death is compensated for by reduction of feedback inhibition. The price to pay is a significantly enhanced level of stem cell division, which could sharply increase stem cell mutagenesis and thus the incidence of cancer. Moreover, if the virus impairs cell function (Butel, 2000) such that feedback factors are produced at reduced levels, then excessive tissue growth is

observed, i.e. the organism develops cancer as a result of the disrupted feedback mechanisms by the virus. Therefore, it is likely that the optimal design (i.e. favored by selection) is the one where feedback factors are produced by both stem and differentiated cells at relative levels that optimize this tradeoff. The notion that in the context of tissue design there is a tradeoff between protection against pathology and protection against excess proliferation during infection provides a new perspective for understanding how tissue architecture relates to function.

It is clear that there is an important connection between viral infections and cancer (Butel, 2000, Damania, 2007, Elgui de Oliveira, 2007 and Helt and Galloway, 2003). Viruses can carry oncogenes (Tarbouriech et al., 2006) and they are thought to induce cancer by causing mutations, typically by inserting themselves into the genome of the host (Helt and Galloway, 2003). Our model suggests a different mode of virus-induced carcinogenesis that does not rely on the generation of mutations in the cells (Banerjee et al., 2010). If the virus simply impairs cell function such that feedback factors in infected cells are not produced, then the corruption of this feedback itself can lead to unbounded cellular growth as long as the virus is present.

This brings us to a caveat. If the basic reproductive ratio of the virus is greater than one, a persistent infection is established and the virus will remain in the host forever in the model. In this way, the growth of a tumor can be continuously driven by the corruption of feedback factor production. Our model does not include immune responses to infection, since this is beyond the scope of the current study. If immune responses are mounted, viral infections can potentially be cleared, as is the case for many infections. If a virus that is

eventually cleared impairs production of feedback factors, then the resulting cellular growth will only be temporary and stop once the infection has been removed by the immune system. In this case, whether the overabundance of cells persists in the long term depends on whether stem cells are infected or not. If stem cells are infected and can be removed by the immune system, the number of cells can be brought back to homeostatic levels. If only differentiated cells are infected, the excess stem cell population that resulted from proliferation cannot be removed because they are not visible to the immune system. In either scenario, the growth that occurred during the presence of the infection can significantly promote accumulation of mutations due to the relatively large number of cell divisions, thus increasing the chances of genetic transformation. There are many viruses that establish persistent infections and that are not cleared, a large fraction of which is probably unknown because they do not cause any overt symptoms. Such viruses could pose an oncogenic danger if they interfere with feedback factor production in infected cells, even if they cannot genetically transform cells.

Methods

The results reported in this paper are based on the analysis of ordinary differential equations (ODEs). They were analyzed by a combination of analytical and numerical techniques. Numerical simulations were performed with Matlab, using the Runge-Kutta 4th order ODE solver. In the simulations, parameters were chosen for illustrative purposes only. Currently, the parameters connected to feedback-mediated tissue regulation are not

known, so measured parameters cannot be used. In addition, the paper is conceptual in nature rather than describing the dynamics of one particular virus infection.

References:

Anderson, R.M., and R.M. May. 1991. Infectious Diseases of Humans. Oxford: Oxford University Press.

Banerjee, P., L. Crawford, E. Samuelson, and G. Feuer. 2010. Hematopoietic stem cells and retroviral infection. Retrovirology 7:8

Butel., J.S. 2000. Viral carcinogenesis: revelation of molecular mechanisms and etiology of human disease. Carcinogenesis 21:405–426

Crosnier, C., D. Stamataki, and J. Lewis. 2006. Organizing cell renewal in the intestine: stem cells, signals and combinatorial control. Nature Review Genetics, 7:349–359

Daluiski, A., T. Engstrand, M.E. Bahamonde, L.W. Gamer, E. Agius, S.L. Stevenson, K. Cox, V. Rosen, and K.M. Lyons. 2001. Bone morphogenetic protein-3 is a negative regulator of bone density. Nature Genetics, 27:84–88

Damania, B. 2007. DNA tumor viruses and human cancer. Trends in Microbiology, 15:38–44

Elgjo, K. and K.L. Reichelt. 2004. Chalones: from aqueous extracts to oligopeptides. Cell Cycle 3:1208–1211

D. Elgui de Oliveira, D. 2007. DNA viruses in human cancer: an integrated overview on fundamental mechanisms of viral carcinogenesis. Cancer Letters 247:182–196

Helt, A.M. and D.A. Galloway. 2003. Mechanisms by which DNA tumor virus oncoproteins target the Rb family of pocket proteins. Carcinogenesis 24:159–169

R.D. Holt. 1977. Predation, apparent competition and the structure of prey communities. Theoretical Population Biology 12:197–229

Lander, A.D., K.K. Gokoffski, F.Y. Wan, Q. Nie, A.L. Calof. 2009. Cell lineages and the logic of proliferative control PLoS Biology, 7:e15

Lo, W.C., C.S. Chou, K.K. Gokoffski, F.Y. Wan, A.D. Lander, A.L. Calof, and Q. Nie. 2009. Feedback regulation in multistage cell lineages. Mathematical Bioscience and Engineering 6:59–82

McPherron, A.C., A.M. Lawler, S.J. Lee. 1997. Regulation of skeletal muscle mass in mice by a new TGF-beta superfamily member Nature 387:83–90

Nowak, M.A., and R.M. May. 2000. Virus Dynamics: Mathematical Principles of Immunology and Virology. Oxford: Oxford University Press

Perelson., A.S. 2002. Modelling viral and immune system dynamics. Nature Reviews Immunology 2: 28–36

Rodriguez-Brenes, I.A., N.L. Komarova, and D. Wodarz. 2011. Evolutionary dynamics of feedback escape and the development of stem-cell-driven cancers. Proceedings of the National Academy of Sciences, USA 108:18983–18988

Tarbouriech, N., F. Ruggiero, M. de Turenne-Tessier, T. Ooka, and W.P. Burmeister. 2006. Structure of the Epstein-Barr virus oncogene BARF1. Journal of Molecular Biology, 359:667–678

Tzeng, Y.S., H. Li, Y.L. Kang, W.C. Chen, W.C. Cheng, D.M. Lai. 2011. Loss of Cxcl12/Sdf-1 in adult mice decreases the quiescent state of hematopoietic stem/progenitor cells and alters the pattern of hematopoietic regeneration after myelosuppression Blood 117:–439

Wu, H.H., S. Ivkovic, R.C. Murray, S. Jaramillo, K.M. Lyons, J.E. Johnson, and A.L. Calof. 2003. Autoregulation of neurogenesis by GDF11. Neuron 37:197–207

Yamasaki, K., N. Toriu, Y. Hanakawa, Y. Shirakata, K. Sayama, A. Takayanagi, M. Ohtsubo, S. Gamou, N. Shimizu, M. Fujii, K. Miyazono, and K. Hashimoto. 2003. Keratinocyte growth inhibition by high-dose epidermal growth factor is mediated by transforming growth factor beta autoinduction: a negative feedback mechanism for keratinocyte growth. Journal of Investigative Dermatology 120: 1030–1037

Zur Hausen, H. 2009. The search for infectious causes of human cancers: where and why. Virology 392:1–10

Chapter 3: An agent-based model of HIV coinfection

Introduction

Mathematical modeling of virus dynamics has yielded key insights into the principles that govern the in vivo spread of viral infections through target cell populations (Nowak and May 2000; Perelson 2002). A relatively unexplored topic in the field of virus dynamics is multiple infection, or coinfection- the simultaneous infection of target cells with more than one copy or strain of a given virus. An important consequence of coinfection is the probability of an increased burst size in coinfected cells, i.e. an increased viral output over the lifespan of multiply infected cells compared to singly infected cells. There are several mechanisms by which coinfection may lead to increased viral output, including recombination leading to fitter genotypes, activation of latently infected cells, and viral complementation. (See Wodarz and Levy 2011 for a detailed discussion of the effects of multiple infection on the dynamics of viral evolution and escape.) Previous modeling work has shown that an increased burst size in multiply infected cells can have profound consequences on the outcome of viral infections (Cummings et al., 2012), and we wish to further this work by investigating how multiple infection influences the dynamics of infection spread in a spatially-structured system.

Traditionally, mathematical models of viral infection assume that a single free virus infects a host cell. However, recent in vitro and ex vivo studies clearly indicate that it is possible for multiple virions to infect a single target cell (Hubner et al., 2009; Levy et al., 2004; Del Portillo et al., 2011). This multiple infection of target cells is a critical mechanism

by which genetic recombination is achieved, as it is the only way to bring multiple strains of a virus in contact with one another inside a host cell (Jung et al., 2002). In particular, studies of human immunodeficiency virus (HIV) have demonstrated that the multiple infection of CD4+ T cells, the natural target of HIV, can occur in local microenvironments through cell-mediated formation of virological synapses that allow for the direct and efficient transfer of up to thousands of virus particles from donor to target cell (Sattentau, 2008; Chen et al., 2007). Cell-mediated transfer of virus has been well documented in other viral infections as well, a notable example being human T cell leukemia virus- type 1(HTLV-1), which relies almost exclusively on the cell-mediated transfer of virus in order to infect new cells (Igakura et al., 2003). In the case of HIV, it has been proposed that the direct transfer of virus represents a mechanism by which the virus evades exposure to neutralizing antibodies (Jolly, 2011; Hubner et al., 2009). While the relative contributions of cell-free and cell-associated viral transfer to the overall spread of infection are not yet known, previous mathematical modeling indicates that the two types of transfer contribute roughly equally to the spread of infection in vitro (Komarova et al., 2013). Despite the importance of cell-mediated transfer to the progression of viral infection, much remains unknown about the principles that govern this process.

One of the major barriers to understanding the evolutionary dynamics of viral infections is that the majority of virus-host interactions in the body cannot be observed directly, and these interactions vary extensively according to the local microenvironment within a tissue type as well as the particular composition of the immune cell types within a tissue (Douek et al., 2003). One particular challenge with HIV has been attempting to characterize the role that coinfection plays in the establishment of new infections in

lymphatic tissues as the virus is disseminated throughout the body. Lymphatic tissues are known to be a major reservoir where new virus is produced, stored, and released into the peripheral blood (Fauci et al 1996; Haase 1999). Cell-mediated viral transfer requires close proximity between donor and target cell for many minutes at a time, and such conditions are only met in somewhat static tissue environments (such as lymph tissue, thymus, and the spleen) they are unlikely to occur in the peripheral blood, where cellular adhesion is counteracted by a high flow rate. Accordingly, coinfection events should be most efficient, and occur most frequently, in tissues with a static or semi-static structure.

Multiple infection is of critical interest to an increased understanding of the underlying dynamics of viral replication and spread in vivo. In this study, we will explore an agent-based model (ABM) that allows us to simulate the local microenvironments of target cells in both tissue and peripheral blood, and investigate the consequences of multiple infection, as well as an increased burst size in multiply infected cells, on the dynamics of early viral spread. The goal is to achieve a better understanding of the role that coinfection plays in the early stages of disease progression, by identifying how infection establishment and outcomes are influenced by multiple infections of target cells. This will be done by comparing the outcomes of a mass-action type cellular environment to those of a spatially structured environment of equal size. We hypothesize that in environments where cell movement is spatially limited and the conditions for sustained cell-to-cell contact are possible, viral coinfection will fundamentally alter the infection dynamics predicted by models that do not account for the possibility of increased output in multiply infected cells.

Results

We begin by describing a basic model of virus dynamics for an agent-based model. The model consists of an NxN square grid, with each space containing either an uninfected cell denoted T, an infected cell denoted I, or nothing. In this model, viral infection spreads according to the law of mass action, with "perfect mixing" of all infected and uninfected cells. According to this rule, each infected cell has an equal probability of infecting any other cell in the grid, and so the radius of infection is equal to N, the length of the grid. Infected cells have a corresponding rate of infection, denoted β.Infected and uninfected cells die according to their respective death rates, where the death rate of infected cells is assumed to be greater than that of uninfected cells. In addition, all cells in this model are singly infected, as we will only consider multiple infection events later on. These conditions approximate the cellular environment found in the peripheral blood, where flow is high and cell-to-cell contact is limited. We do not track free virus directly, as it can be assumed to be proportional to the number of infected cells (see Nowak and May 2000). While the assumptions underlying this simplified scenario are likely to be violated, it allows for a direct comparison of the ABM model with differential equation models whose solutions can be determined analytically. Under perfect mixing conditions, the ABM model can be described by the following ordinary differential equation (ODE) model, a classic predator-prey model that has been described previously (Nowak and May 2000; Perelson 2002). In this model the population of infected cells, I, is generated from uninfected cells, T:

(Eqn. 3.1)

$$\frac{dT}{dt} = L - dT - \frac{BTI}{k}$$

$$\frac{dI}{dt} = \beta TI/k - aI$$

In this model, k is equal to the total grid size, i.e. $NxN = k$. L is an input term that represents the production of new uninfected cells. Infection of target cells occurs with rate β, and a successful infection generates one new singly infected cell. The death rates of uninfected and infected cells are denoted by d and a respectively, with the assumption that $a > d$ in all scenarios, i.e. infected cells have a higher death rate than uninfected cells. Note that the infection term, $\beta TI/k$**,** is a simple logistic function- infected cells grow exponentially when the total number of infected cells is low, and eventually saturate at some equilibrium level. This behavior is shown in Fig. 3.1, which compares ABM and ODE outcomes for an NxN grid with $N = 100$ and $k = 10{,}000$ (model parameters and initial conditions are kept constant across simulations).

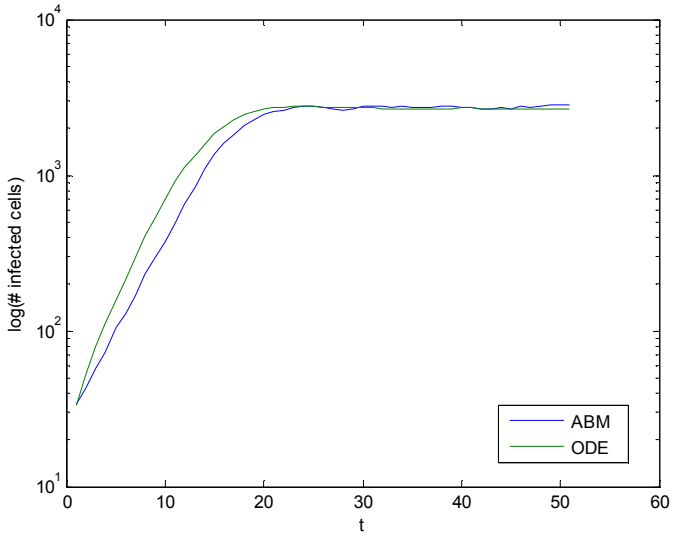

Fig 3.1 Outcomes of ODE and ABM model are roughly the same for the simplest case scenario where perfect mixing of cells occurs. Parameters are as follows: $d = 0.02, a = 0.01, \beta = 0.05, L = 0.1$ Initial conditions=36 infected cells.

Now we wish to explore the model under the assumption that any given cell can become infected with more than one virus particle, resulting in a cell containing up to *n* total virus particles and an *n*thly infected cell. If we assume that multiply infected cells are present, we can then further assume that viral cooperation in multiply infected cells- leading to an increased burst size- is either present or absent.

We will first address coinfection assuming there is no viral cooperation. In the absence of any cooperative effects that increase viral output in multiply infected cells, the model outcomes reduce to the those of the previous non-cooperative mass action model- cells grow exponentially at low viral loads, with the sum of all infected cells-from singly to *n*thly infected-equal at steady state to the singly infected cell population from the simplest case scenario (not shown).

Next, we will explore the model under the assumption that there is some degree of viral cooperation present in multiply infected cells. This is formulated in the model by an increased viral output in any cell containing two or more virions. In the first part of the investigation we will assume that two viruses per cell are sufficient for complementation and/or cooperation to occur, but this increased burst size is constant- it does not increase with any further multiplicity of infection (this alternative scenario will be discussed later on). The outcome of an increase in burst size for multiply infected cells is shown in Fig. 3.2 for the mass-action scenario, where the radius of infection for a given cell is not limited.

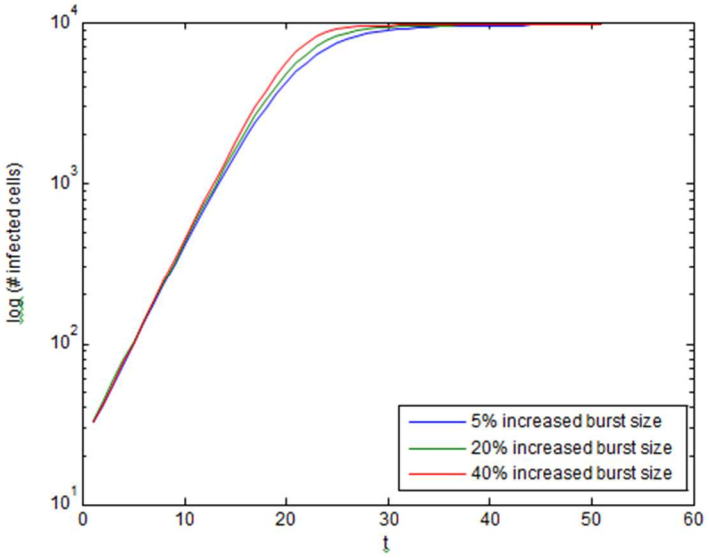

Fig. 3.2 Outcome of agent-based model under perfect mixing conditions when an increased burst size in multiply infected cells is accounted for. Early viral load is unaffected by increased burst size. Parameters are as follows $d = 0.001, a = 0.01, \beta = 0.3, L = 0.1$

An increased burst size in multiply infected cells does not fundamentally alter the exponential growth pattern of infected cells, and growth at low viral loads is nearly identical for different burst sizes. The explanation for this outcome is that in a perfectly mixed system, coinfection events are rare when infected cells are rare, as the likelihood of infecting an already infected cell becomes very small. Although multiply infected cells are expected to increase the rate at which infection spreads, they make up only a small proportion of the total number of infected cells in the early stages of infection. A slightly increased infection rate is only observed at higher viral loads, when the infection has spread through the system and a modest population of coinfected cells has been generated.

In order to investigate coinfection under conditions where space and mixing are limiting to cellular interactions, we will next add a "nearest-neighbor" rule that assumes infected cells can only spread infection to nearby targets. Each infected cell has a given

radius, r, of cells which it is capable of infecting, and cells outside this radius cannot be infected. In the most limiting nearest-neighbor case, where $r = 1$, there are 8 possible target cells for each infected cell. When $r = k$, the length of the grid, there is no restriction to cellular interactions and the model reduces to the mass action outcome. At an intermediate radius (eg. $r = 3$) we expect outcomes to demonstrate properties that are intermediate between mass action and nearest-neighbor type simulations.

Outcomes for the nearest neighbor model are shown in Fig. 3.3 for an intermediate radius of infection case, with $r = 2$. The plot includes outcomes for a model of coinfection with and without cooperation. Model parameters and grid size are identical to all previous mass action simulations. A log plot is shown in Fig. 3.3a, followed by square root plot in Fig. 3.3b to demonstrate the pattern of surface growth.

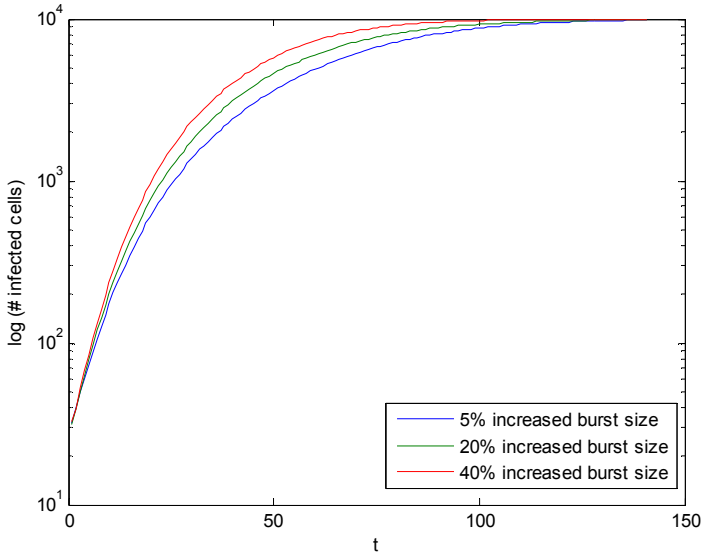

A

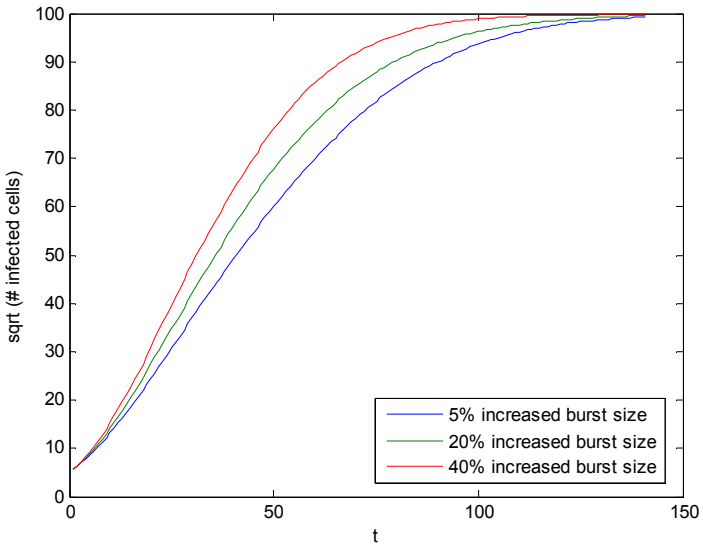

B

Fig. 3.3 Outcome of agent-based model for an intermediate radius of infection, r=2. Infection spreads according to the square of the total number of infected cells (Fig. 3.3b) indicating surface growth. In addition, an increased burst size in multiply infected cells leads to acceleration in the spread of the infection relative to the scenario where no increased burst size is considered. Parameters are as follows $d = 0.001, a = 0.01, \beta = 0.3, L = 0.1$

Notice that the growth of infected cells in the nearest neighbor simulation is roughly linear in the square root plot. This pattern is indicative of surface growth, where the growth is proportional to the square root of the current number of infected cells. Recall that for low viral loads, the mass action model of coinfection predicts an exponential growth rate for infected cells, one that is unaffected by the addition of cooperative interactions. This can be attributed to the rarity of coinfection at low viral loads, and an infected cell population dominated by singly infected cells. If any degree of spatial limitation is imposed on the spread of infection, however, the relative proportion of multiply infected cells to singly infected cells at low viral loads is dramatically increased with the addition of viral cooperative effects. See figure 3.4 for simulations that include modest cooperative viral interactions for both a mass action and nearest-neighbors simulation. The reason for this

outcome is as follows. At low viral loads, infected cells in a nearest neighbor system will begin to infect a small pool of nearby cells, and coinfection events are more common when the number of possible targets is low. As coinfection events occur more rapidly in this system, multiply infected cells will make up a large fraction of the infected cell population after only a short time in nearest-neighbor conditions. This is in contrast to the mass action simulations, where singly infected cells dominate at low viral loads.

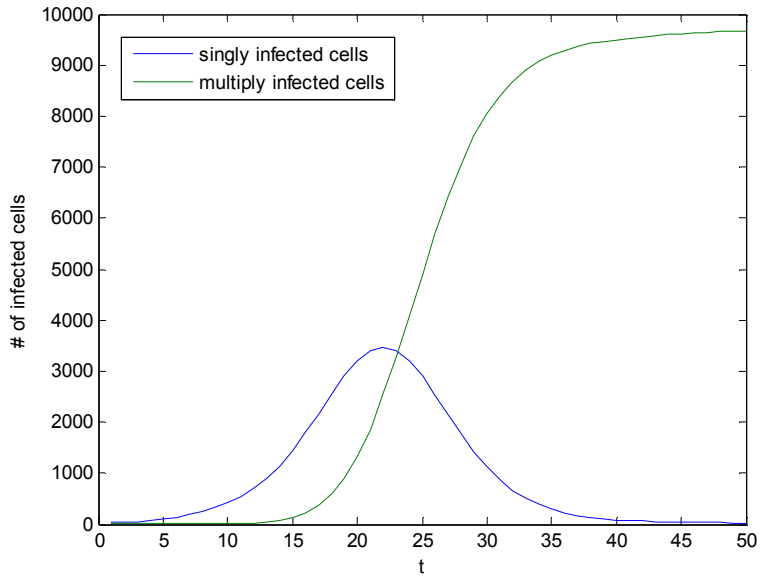

A

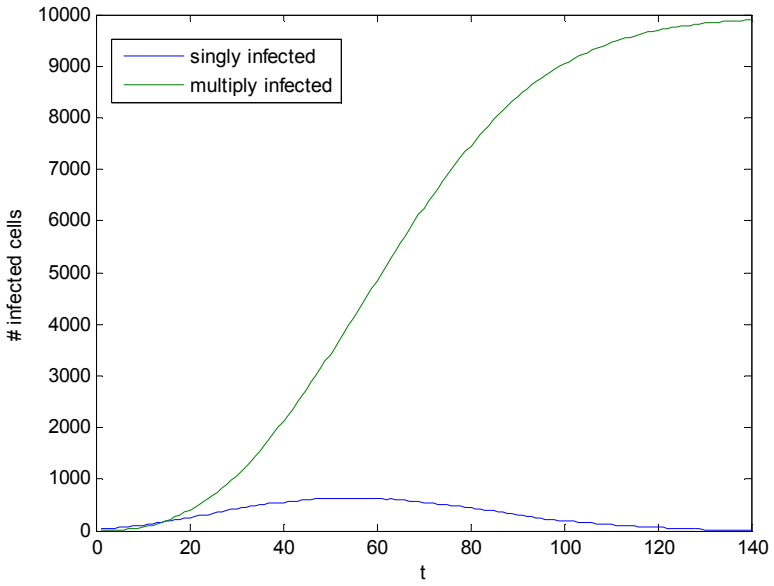

B

Fig. 3.4 Model outcomes for perfect mixing (Fig. 3.4a) and nearest neighbors (Fig. 3.4b) simulations with a 10% increased burst size in multiply infected cells. The proportion of cells that are multiply infected at low viral loads is much larger in the nearest neighbors setting relative to the perfect mixing scenario. Parameters are as follows $d = 0.001, a = 0.01, \beta = 0.3, L = 0.1$

This property can also be described as an increase in the average burst size of infected cells as the overall proportion of multiply infected cells increases.

A large proportion of coinfected cells at low viral loads can have several consequences on the spread of infection. Coinfection can act as a "boost" to the establishment of infection by driving up the overall infection rate of the infected cell population. Simulations in an intermediate mixing neighborhood indicated that even a relatively modest 5% increase in the burst size of multiply infected cells can provide such a boost (Fig. 3.6).

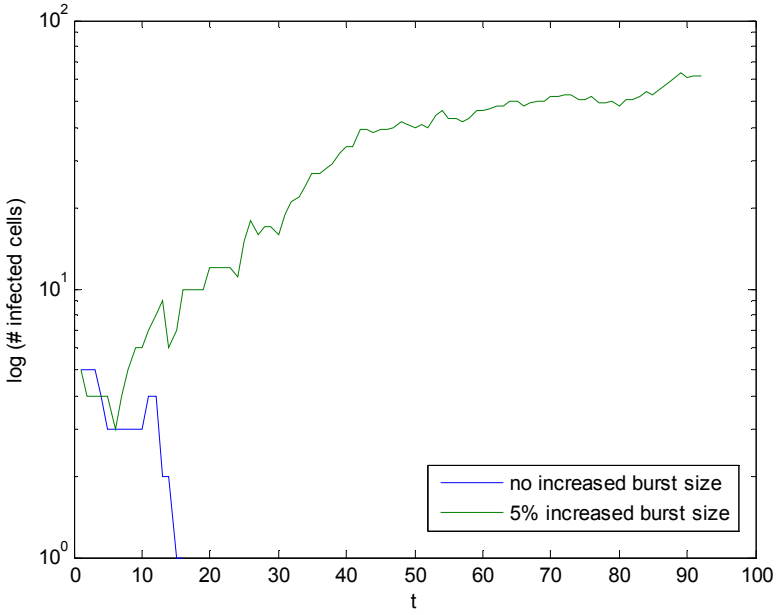

Fig 3.5 Outcome of infection under initial conditions where establishment of infection is not certain. Infection fails to establish in the model where no increased burst size in multiply infected cells is considered, at an intermediate infection radius of r=5. Under identical conditions, a small increased burst size in multiply infected cells can lead to establishment of infection. Parameters are as follows $d = 0.001, a = 0.01, \beta = 0.3, L = 0.1,$ Initial number of infected cells = 4.

We wanted to understand how the relationship between initial viral load and likelihood of an infection becoming established would be influenced by an increased burst size in multiply infected cells. We compared these outcomes at several different initial infection sizes, ranging from a single initially infected cell to 25 initially infected cells. The extinction rate of the infection under each set of initial conditions was found. These simulations were explored in the strictest nearest neighbor settings, with r=1. Outcomes are shown in Fig. 3.7, for simulations with 1, 4, 9, or 25 initially infected cells, with a 5% increased burst size in multiply infected cells.

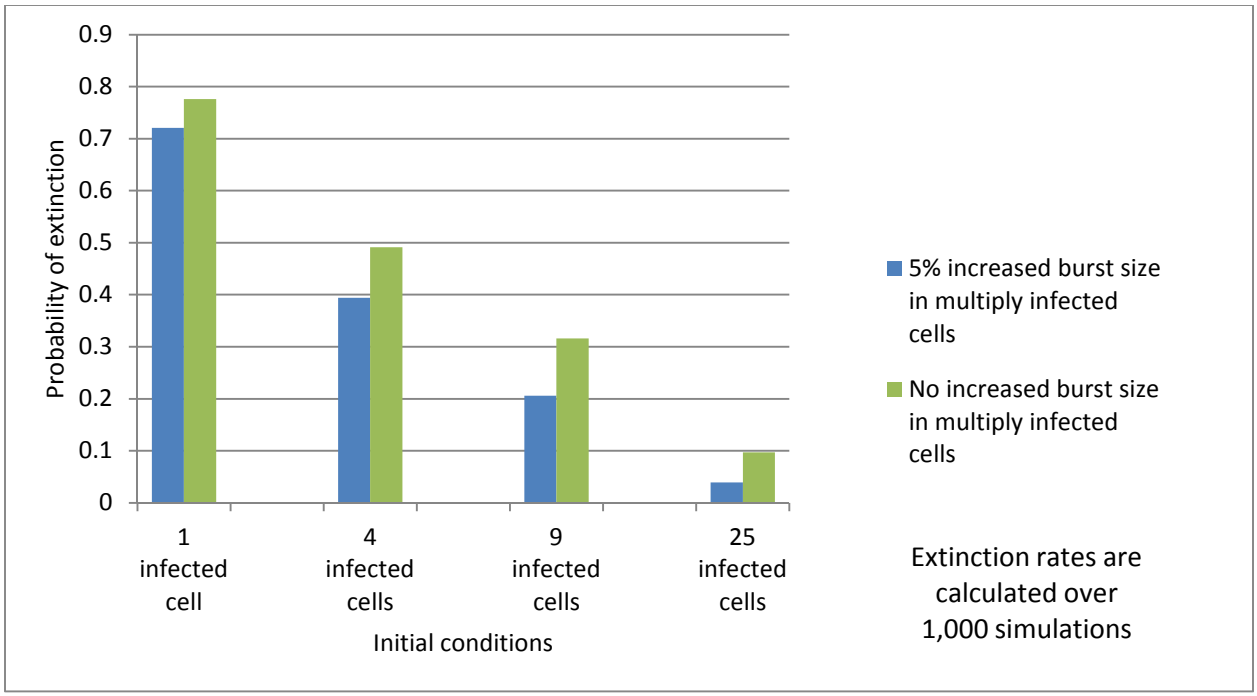

Fig 3.7 Probability of infection extinction for initial conditions ranging from one initially infected cell to 25 initially infected cells. Accounting for an increased burst size in multiply infected cells leads to a decreased probability of infection extinction for all initial conditions. Parameters are as follows d=0.001, a=0.06, β= 0.1, L=0.1, r=1.

A larger initial infection size correlates with a lower probability of extinction in both models, which is intuitive. When an increased burst size for multiply infected cells is included in the model, a lower extinction rate is predicted relative to the basic model. This indicates that under conditions where spatial mobility is limited, the establishment of infection is greater when multiply infected cells are present. This is in agreement with previous experimental work in temporal tracking of adenovirus plaque formation that suggests that establishment of infection is higher when multiply infected cells arise immediately upon infection (Hofacre et al., 2012).

Finally, we will introduce a property of infection known as viral synapsing. Viral synapsing involves the formation of a synaptic bridge between two T cells, at least one of which is already infected, and the transfer of cytoplasmic virions from host to target cell.

The benefit of synapse formation is that it provides a mechanism by which cell-associated virus can infect new targets with a transfer rate of anywhere from 10-18,000x efficiency over free virus transmission (Chen, et al., 2007). While viral synapsing has been proposed as an essential process to the establishment and spread of HIV infection within tissues, the relative contributions of free-virus transfer vs. cell-associated virus transfer to the overall spread of infection remain unknown. We will assume only that cells participating in a synapse are unable to simultaneously undergo free virus transfer, and will further assume that the relative rate of synaptic transfer is identical that of free virus transfer, i.e. there is no time cost associated with synapsing. The process of synapsing is modeled by the transfer of a random number of viruses from a donor to target. The target cell may be either uninfected or infected. The minimum number of virions that can be transferred is 1, and the maximum number of virions that can be transferred is V_{max}. The probability of a single virion being successfully transferred along the synapse is denoted $P_{transfer}$.

We will look at synapsing on its own, without the consideration of free virus transfer. The relative amount that free virus and cell-to-cell transfer contribute to total number of infection events is unknown, and so it is of little use to explicitly model the combined case. If the explicit formation of viral synapses is included in the model, the resulting infection growth pattern accelerates as burst size increases and as the efficiency of synaptic transfer (i.e. the relative number of viruses transferred per synapse) increases, as shown in Fig. 3.8 for mass action scenarios.

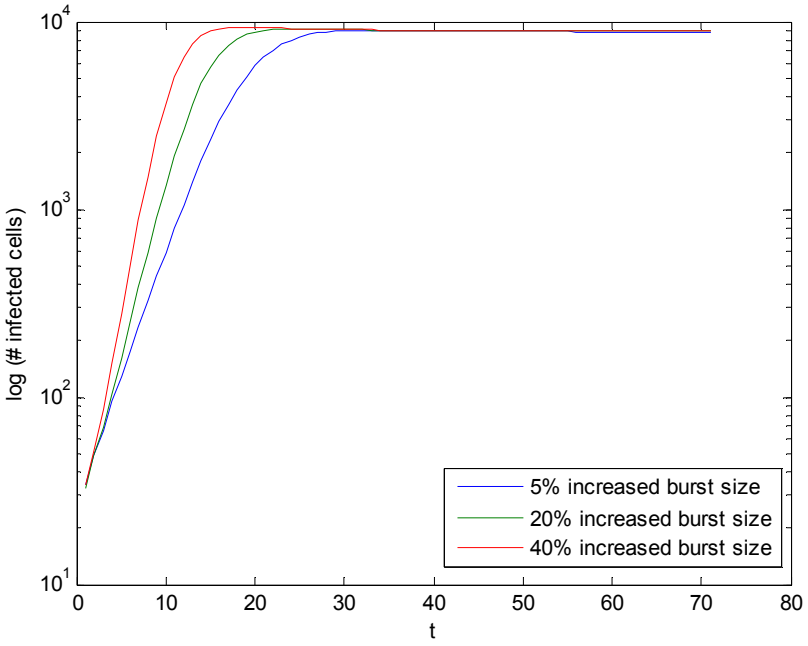

A

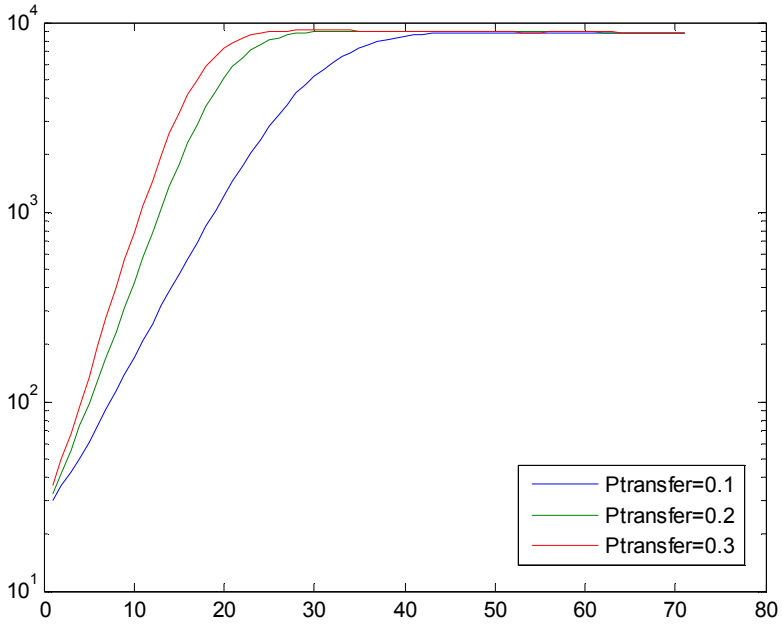

B

Fig. 3.8 Outcome of agent-based model considering synaptic transfer between cells only. In this model, acceleration of infection is observed in a manner similar to the nearest neighbor model. In fig. 3.8b, the probability of a successful transfer event between target and host is varied, with acceleration in growth of infection observed. Parameters are as follows $d = 0.001, a = 0.01, \beta = 0.3,\ L = 0.1$, $P_{transfer}$=0.3 (fig 3.8a), V_{max} =10.

The inclusion of synaptic transfer of virus to the model has the additional effect of increasing the relative amount of multiply infected cells in the overall population of infected cells. As the probability of synapsing is increased, the proportion of multiply infected cells increases relative to the singly infected cell populations. As discussed previously, this increase in the multiply infected cell population at low viral loads will result in an increase in the average burst size of infected cells and acceleration in overall infection growth rate. In essence, viral synapsing results in a similar effect as that of the nearest-neighbor conditions that have been previously discussed, leading to altered infection dynamics that result in a larger population of coinfected cells at low viral loads. This complements the nearest-neighbors results discussed earlier, and suggests that the acceleration of infection observed at different burst sizes will underestimate the number of multiply infected cells generated early on when synapsing is the dominant transfer mode.

These results indicate that the dynamics of viral infection may be profoundly influenced by the properties of the local microenvironment. In regions of the body where cellular migration is limited and cells are mostly static, we find that coinfection events are common and multiply infected cells soon dominate the infected cell population at low viral loads, increasing the overall average replication rate of infected cells. This increases the probability that infection can be established in new locations, and will likely lead to increased recombination events that contribute to immune escape. We find that the inclusion of viral synaptic transfer to the model, making no assumption about spatial limitation, leads to a similar outcome- multiply infected cells are generated in higher proportions at lower viral loads, assuming synaptic transfer is more efficient than free virus transfer, which experimental evidence indicates is likely (Chen et al 2007; Komarova

et al., 2013). This indicates that in local microenvironments where space is limiting and/or the conditions for viral synapsing are present, we can predict a larger population of coinfected cells relative to singly infected cells. As discussed previously, this provides the conditions favorable to viral recombination and complementation, which will likely lead to increased viral output over the course of infection in these multiply infected cells.

It would be of interest to further explore these outcomes in experimental systems where multiple infection is known to occur. Preliminary experiments indicate that an increased burst size in multiply infected cells is likely to occur via viral complementation and other cooperative effects (unpublished experimental data), and further experimental work will allow us to verify whether or not burst size of cells is higher in more spatially structured environments, where multiple infections and viral synapsing are best facilitated.

References:

Chen, P., Hübner, W., Spinelli, M.A., and Chen, B.K. 2007. Predominant mode of human immunodeficiency virus transfer between T cells is mediated by sustained Env-dependent neutralization-resistant virological synapses. J Virol 81(22):12582-95

Cummings, K.W., Levy, D.N., Wodarz, D. 2012. Increased burst size in multiply infected cells can alter basic virus dynamics. Biol Direct 7:16

Del Portillo, A., Tripodi, J., Najfeld, V., Wodarz, D., Levy, D.N., Chen, B.K. 2011. Multiploid inheritance of HIV-1 during cell-to-cell infection. J Virol 85(14):7169-76

Douek, D.C., Picker, L.J., Koup, R.A. 2003. T cell dynamics in HIV-1 infection. Annu Rev Immunol 21:265-304

Fauci, A.S., Pantaleo, G., Stanley, S., Weissman, D. 1996. Immunopathogenic mechanisms of HIV infection. Ann Intern Med 124(7):654-63

Haase, A.T. 1999. Population biology of HIV-1 infection: viral and CD4+ T cell demographics and dynamics in lymphatic tissues. Annu Rev Immunol 17:625-56

Hofacre, A., Wodarz, D., Komarova, N.L., Fan, H. 2012. Early infection and spread of a conditionally replicating adenovirus under conditions of plaque formation. Virology 423(1):89-96

Hubner, W., McNerney, G. P., Chen, P., Dale, B.M., et al. 2009. Quantitative 3D Video Microscopy of HIV Transfer Across T Cell Virological Synapses. Science 323(5922): 1743-47

Igakura T., Stinchcombe J.C., Goon P.K., Taylor G.P., Weber J.N., Griffiths G.M., Tanaka Y., Osame M., and Bangham C.R. 2003. Spread of HTLV-I between lymphocytes by virus-induced polarization of the cytoskeleton. Science 299:1713–1716

Jolly, C. 2011. Cell-to-cell transmission of retroviruses: Innate immunity and interferon-induced restriction factors. Virology 411(2): 251–259

Jung, A., Maier, R., Vartanian, J.P., Bocharov, G., Jung, V., Fischer, U., Meese, E., Wain-Hobson, S., Meyerhans, A. 2002. Recombination: Multiply infected spleen cells in HIV patients. Nature 418(6894):144

Komarova, N.L., Levy, D.N., Wodarz, D. 2013. Synaptic transmission and the susceptibility of HIV infection to anti-viral drugs. Sci Rep 3:2103

Levy, D.N., Aldrovandi, G.M., Kutsch, O., Shaw, G.M. 2004. Dynamics of HIV-1 recombination in its natural target cells. Proc Natl Acad Sci USA 101(12):4204-9

Nowak, M.A., and R.M. May. Virus Dynamics. Oxford University Press, 2000.

Perelson, A.S. 2002. Modeling viral and immune system dynamics. Nature Reviews Immunol 2:28-36

Sattentau, Q. 2008. Avoiding the void: cell-to-cell spread of human viruses. Nat Rev Microbiol 6:815–826

Wodarz, D., and Levy, D.N. 2011. Effect of multiple infection of cells on the evolutionary dynamics of HIV in vivo: implications for host adaptation mechanisms. Exp Biol Med 236(8):926-37